ARC Report No. 86-150

FOS CALIBRATION REPORT

(AV-04)

To

University of California, San Diego
La Jolla, CA 92093

and

NASA/Goddard Space Flight Center
Greenbelt, MD 20771

By

Dr. Richard J. Harms
Applied Research Corporation
8201 Corporate Drive, Suite 920
Landover, MD 20785

March 1986

TABLE OF CONTENTS

1.0 INTRODUCTION

1.1 Scope and Method

This report documents the results of the final FOS instrument-level calibration conducted prior to delivery for integration into the HST. Measurements were obtained both in ambient and under orbital-simulated (thermal/vacuum) conditions. The purposes of the tests can be summarized under two main categories:

1. Verify proper operation of the FOS to meet its CEI Specifications prior to delivery for integration into HST; and
2. Obtain calibration data needed for proper scientific planning, and use as a data base for trend analysis. Any trends already apparent from comparing instrument-level test to prior subsystem-level tests are explicitly discussed in this report.

Descriptions of the test arrangements necessary to understand the results are included here; detailed test procedures are not reproduced in this report, but are available in extensive detail. Similarly, here we describe the test results. The raw data exists on magnetic tape, and a few thousand pages are available in hardcopy for the truly curious.

Finally, this report highlights CEI compliance, deviations, and anomalies. Where performance is less than specified, the impacts are discussed. In some areas, analysis is still under

way; where significant uncertainties still exist in the test analyses, they are explicitly stated in this report.

1.2 Timeline Summary

The instrument-level tests described in this report were conducted at MMDA during Summer 1984, prior to the FOS Pre-Ship Review (PSR) held on September 18, 1984. This report primarily reflects detailed analysis of the test results available in quick-look form at that time. A few exceptions exist, where further data has been obtained to follow up on problems or uncertainties identified at the PSR. Much work has been done, and substantial improvements made, in the area of filter-grating wheel (FGW) repeatability; recent results are included in this report. Also, further target acquisition test results are presented in the appropriate chapter. Finally, any indications of changes in instrument performance as late as March 1985 are noted, even if the data may be only partially complete. Thus, the FOS performance described herein is, as best we know, complete to March 1985, although it must be emphasized that the latest completed set of test data dates to Summer 1985.

After these data were obtained, the red detector was replaced by a spare (in December 1985). No system-level data are yet available. Based on detector measurements for the original and spare red assemblies, we discuss anticipated performance changes for the FOS in Sections 2.1 and 2.2.

2.0 EXECUTIVE SUMMARY

2.1 Major Results

The primary purposes of performing the calibration tests discussed in this document were threefold. First, we wished to discover deficiencies in the FOS and correct them; the results of this purpose are discussed in this section below. Second, we wanted to characterize the performance of the FOS to determine how closely it achieves its performance specifications; Section 2.2 addresses this issue. Finally, we obtained calibration data, some of which can only be obtained in laboratory measurements (such as polarimetry retardation angles), and most of which form a baseline to compare against future ground-based and on-orbit calibrations.

These tests uncovered deficiencies, some of which were major. The most significant instrument deficiency found was the steady deterioration in performance in the original red flight detector. As a result, it was replaced late in 1985 with a spare flight detector nearly, but not quite, as good as the original had been before its deterioration. The expected performance from this new detector is briefly mentioned in Section 2.2. A second major deficiency discovered by these tests was the inadequate repeatability of the filter-grating wheel mechanism compared to the needs of the planned FOS target acquisition procedures. This problem could not be completely eliminated, but was substantially ameliorated through modifying the mechanism stepper-motor sequences, by installing internal LED illumination sources for

use during target acquisition, and by modifying the flight software to allow use of the LED sources to compensate for image movements due to the filter-grating wheel.

Happily, the calibration results principally showed that the FOS will meet most of its design performance requirements. The data obtained were sufficient to derive first-order databases for the STScI calibration files and to allow reasonably realistic planning of GTO (and GO) scientific programs using the FOS. Following the repairs described in the paragraph above, the FOS has been calibrated to be a scientifically useful instrument meeting nearly all the performance requirements discussed in Section 2.2.

2.2 CEI Compliance

The FOS scientific performance requirements are called out in a portion of the Contract End Item (CEI) Specifications Document, summarized in Tables 2.2-1 and 2.2-2 and Figures 2.2-1 and 2.2-2. These requirements are verified (or not) by the calibrations described in this document and are further discussed below.

Items A through D - Instrument Geometry: These requirements were measured at the component level and assured by the geometry of the FOS design. The calibration results are in all cases consistent with the geometrical specifications, but by themself do not directly verify these requirements.

Item E - Spectral Resolving Power: The results given in Section 5.0 verify complete compliance with these specifications.

Item F - Instrument Profile: The results presented in Section 6.5.2 verify only that the required performance is at least

TABLE 2.2-1

INSTRUMENT PERFORMANCE REQUIREMENTS

A. Detectors

The instrument shall contain two independently operable 512-channel digicon detectors with associated electronics.

B. Image Format

Each detector diode array shall be a linear array of 512 elements on 50 μm nominal centers. Each array element shall have a geometric height of 200 ± 10 μm and a geometric width of 40 ± 2 μm.

C. Image Scale

The spectrograph optics shall reimage the entrance aperture focal plane such that the image scale at either detector is 140 ± 10 μm/arcsecond when illuminated by the OTA or its optical equivalent.

D. Fields of View

There shall be 12 apertures with dimensions corresponding to fields of view from 0.1 arcsec to 4.3 arcsec in scale. The size, configuration and relative locations of the apertures are defined in Table 2.2-2. Apertures not selected for a given observation shall not allow stray light contamination. One aperture position shall be opaque. A failsafe position shall be provided with 0.5 arcsec and 4.3 arcsec square apertures.

E. Spectral Resolving Power

When observing a point source, the instrumental profile full spectral width at one-half peak response, divided into the source wavelength at the center of each spectral subrange, shall be 1000 + 500, -0 for the high resolution modes, and shall be 200 ± 50 for the low resolution modes.

F. Instrument Profile

When observing a point source, the instrument profile (defined as the detector response to a monochromatic source from within a solid angular distribution simulating the OTA focal ratio, central obscuration, and astigmatism) for every resolution mode and spectral range, when normalized to peak response = 1.0 shall lie on or below the curve depicted in Figures 2.2-1 and 2.2-2 for every detector diode.

G. Spectral Ranges

The FOS optical geometry shall permit observations with a spectral resolving power of 1000, as defined above, over a wavelength range from 114 to 900 nm. The optical geometry shall permit observations with a spectral resolving power of 200, as defined above, over the range from 114 to 800 nm. The optical geometry shall permit spectropolarimetric observations over a wavelength range from 120 to 320 nm, and a non-dispersive train for direct imaging from 114 to 900 nm. Order blocking filters shall be included that provide transmission linear with wavelength and constant within +/-1% over the range 319 nm to 800 nm within the clear aperture.

H. Efficiency

For both the resolution = 1200 and 200 modes as described above, FOS efficiency shall: exceed 1.0 percent over the entire range from 120 nm to 700 nm; exceed 2.0 percent from 120 to 200 nm; exceed 7.0 percent from 200 to 400 nm; and shall have a peak efficiency exceeding 10.0 percent.

I. Instrument Noise

The FOS background noise from all sources during inflight operating conditions outside the SAA shall not exceed 2×10^{-3} counts/sec/diode at -10^{o}C photocathode temperature.

J. In-Flight Calibration

The FOS shall have on-board spectral calibration sources to allow determination of any astronomical source apparent wavelength to a relative accuracy of 20 percent of the spectral resolution at that wavelength, and it shall have a flat-field source.

K. Exposure Intervals

The FOS shall be capable of exposure times of 3 milliseconds minimum duration, shall be capable of meeting performance requirements with minimum intervals of 18 milliseconds between exposures and shall be capable of maximum continuous exposure rates up to thirty three 512-channel exposures/second.

L. Instrument Stability and Repeatability

The FOS radiometric response (total counts per photon for a monochromatic input to the instrument) derived from repeated measurements shall be constant within the following limits for 99 percent of the operating diodes.

1) The response shall be stable to within 1.0 percent over periods up to 4 hours with the opto-mechanical configuration held constant.

2) The response shall repeat within 3.0 percent for opto-mechanical reconfigurations (returning to starting configurations) during a 4-hour observing period.

3) After achieving thermal equilibrium, response shall repeat within 8.0 percent for measurements made up to 24 hours apart (with the opto-mechanical configuration returned to that of the first measurement, with the instrument recalibrated with the internal wavelength calibration system and with the target recentered with the ST).

M. Pulse Saturation Error Correction

For input count rates randomly distributed in time up to 10^5 counts/sec/diode, the measured rate shall be correctable to the true input rate to a precision better than 4.0 percent. For input rates (also random in time) between 1 and 10^4 counts/sec/diode, the measured rate shall be correctable to the true input rate to an accuracy better than 1.0 percent.

N. System Switching Time

The time required for the FOS to switch from operation with one detector to operation with the other detector shall not exceed 5 minutes for the target acquisition aperture and 30 minutes for the A-4 aperture.

O. Acquisition

When provided with an input image of a point light source with position stability better than 0.01 arcsec, the FOS shall be able to locate its centroid to within ±0.03 arcsec for use in target acquisition.

P. The photocathode operating temperature shall be maintained between $-32^{\circ}C$ and $-8^{\circ}C$ for the cold and hot interface sink temperature extremes defined in ST-ICD-02, Axial SI to OTA/SSM.

Q. Polarimeter Optics

The FOS shall be equipped with a polarizer module which shall modulate the light irradiance on the detector in a way related to the state of polarization of the incident light. In particular, the modulation of the irradiance shall exceed seventy percent (70%) for 100% linearly polarized input light of any position angle for wavelengths from 121.6 to 300 nm. The polarizer module shall have a transmission of unpolarized light exceeding 0.1 at 121.6 nm when both output beams are summed. The polarizer module shall have a setting so that both FOS beams are clear simultaneously. In the event of failure of the polarimeter, it shall be possible to remove it from the light paths permanently.

R. Derived Limiting Magnitude (Informational Purpose Only - Not an Additional Requirement)

From the FOS efficiency and noise performance stated in 3.2.1.H and 3.2.1.I, and assuming an OTA collecting area of 4.5 x 10^2 cm^2 with 63% OTA throughput, the FOS will achieve S/N > 7 per diode at 400 nm in the $\lambda/\Delta\lambda$ = 1200 mode for a 3-hour integration of an unreddened A0V stellar flux distribution of magnitude V = 23.

S. Mechanism Uncompensated Momentum

The mechanisms' uncompensated momentum shall be controlled to minimize jitter of the stellar image.

TABLE 2.2-2

APERTURES AND RELATIVE POSITIONS

GROUP	NO.	SIZE (WxL)* (ARC SEC)	NUMBER	SHAPE	PURPOSE
B	1	0.5	Single	Round	Science-Polarization
	2	0.3	Single	Round	Science-Polarization
	3	1.0	Single	Round	Science-Polarization
	4	Blank	--	--	Background
A	1	4.3	Single	Square	Acquisition
	2	0.5	Paired	Square	Science-Beam Switching
	3	0.25	Paired	Square	Science-Beam Switching
	4	0.10	Paired	Square	Science-Beam Switching
C	1	1.0	Paired	Square	Science-Beam Switching
	2	0.25 x 2.0	Single	Rectangular	Science-Nebular
	3	2.0	Single	Square	Science-Wide Occulter (0.3 arcsec bar)
	4	0.7x2.0	Single	Rectangular	Science-Narrow Occulter (0.3 arcsec bar)

*W(width) in-dispersion
L(length) cross-dispersion

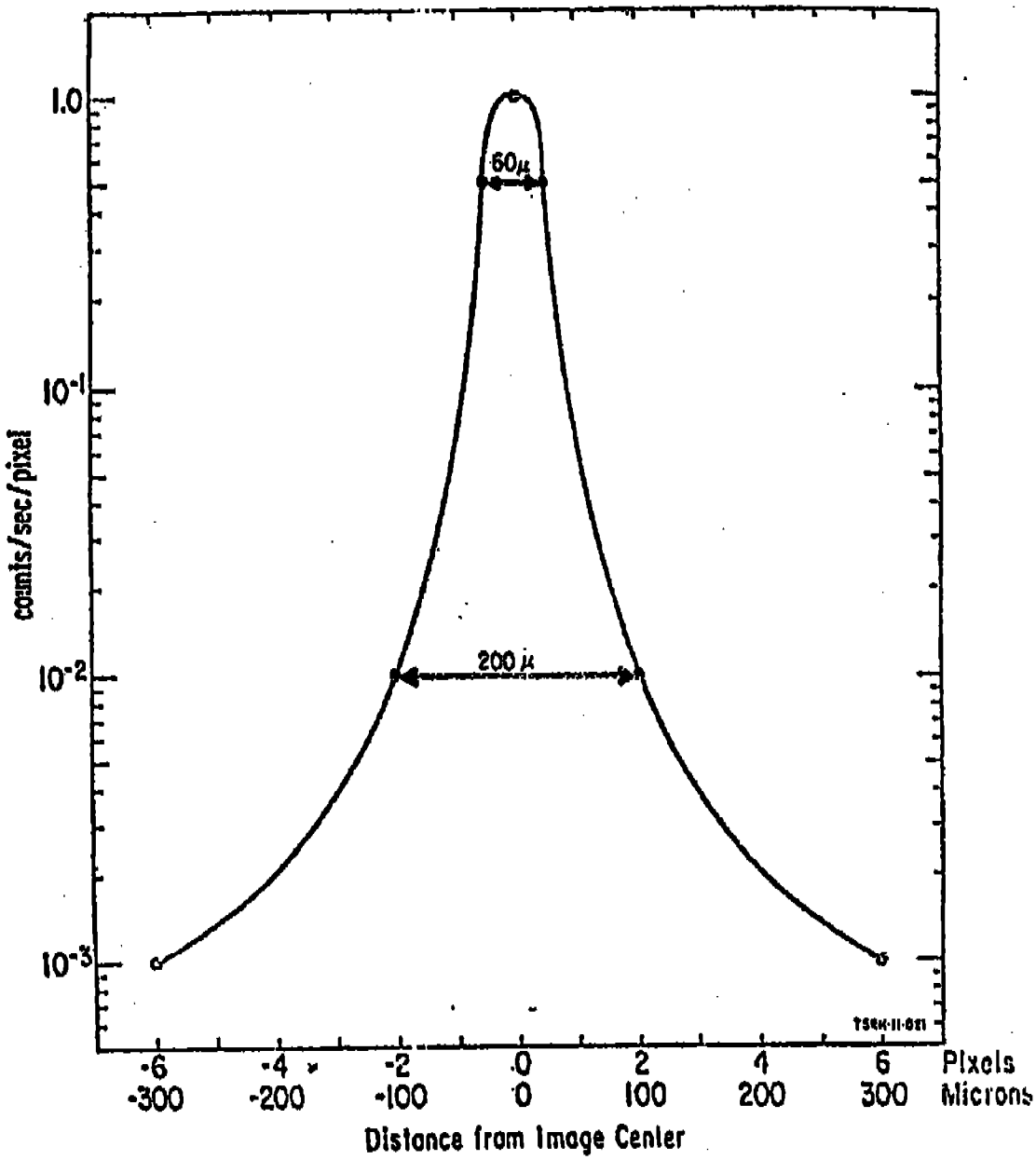

Figure 2.2-1. FOS Instrument profile distance from Central Image Point $\leq$ 6 pixels

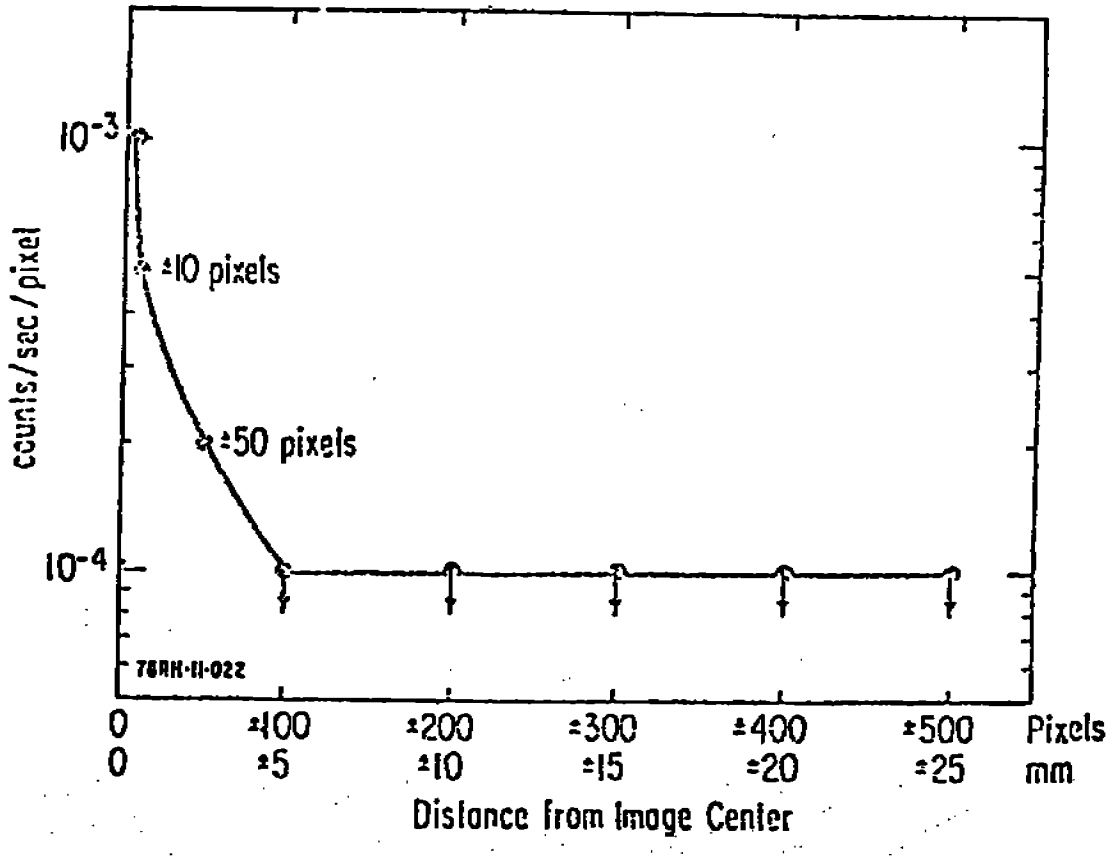

Figure 2.2-2. FOS instrument profile distance from central image point ≤ 6 pixels

nearly met. The near-field and far-field requirements are fully met, but the mid-field (2 to 20 diodes off line-source) requirement may not be met by as much as a factor of two in the permitted scattered light. The calibration results provide only upper limits to actual FOS scattered light performance, so the results do not prove the full specification is not met, merely they fail to prove conclusively that the mid-field performance is met. Fortunately, the worst-case profiles derived in Section 6.5.2 assure good scientific utility for the spectrograph with performance adequate to carry out the intended observational programs.

Item G - Spectral Ranges: The results of Section 5.1 verify that these requirements have been met. Note, however, that as discussed below, the red response makes most observations infeasible for wavelengths much longward to 800 nanometers.

Item H - Efficiency: Measurement of the instrument absolute photometric efficiency, described in Section 6.2, was by far the most difficult of the calibrations performed. The initial results indicated clearly that the specifications were not being met and discovered deterioration in the red flight detector which led to its being replaced. Although instrument-level calibrations have not been performed after the detector replacement, the results of Section 6.2 can be scaled from the results of the detector efficiencies obtained for each of the flight detectors. Within the measurement uncertainties, often as large as 25%, the FOS with the original detectors, met the requirement of 1% efficiency from 120 to 700 nm. With the replacement red detector, the upper end of this range is in doubt, and the limit of 1%

throughput may lie as low as 660 nm. Further system-level measurements are planned, but in view of the difficulty in obtaining absolute accuracies better than around 20%, the exact threshold of 1% efficiency may remain uncertain in the range 660 to 700 nm. The requirement that efficiency exceed 2% from 120 to 200 nm is substantially verified, although the accuracy of the measurements below 130 nm is not excellent. The remaining requirements are not met; the efficiency in the resolution = 1200 mode between 20 and 400 nm is 5% to 6%, rather than the specified 7%, and the peak resolution = 1200 efficiency is near 7%, not 10% as specified. Similarly, the mode resolution = 200 efficiencies fail to meet specifications, with the actual efficiency running from 4% to 9% in the 200 to 400 nm range, and the peak efficiency reaching nearly 9% (almost the specified 10%) around 350 nm. Although the instrument does not completely achieve the specified efficiencies, it does come close to them throughout the entire spectral range, and so will be able to achieve substantially all its science objectives, but at the cost of somewhat (20% to 40%) greater observing times being required.

Item I - Instrument Noise: The results given in Section 6.5 and the detector measurements on the replacement red detector verify that the FOS completely meets these requirements with some margin to spare.

Item J - In-Flight Calibration: From the results in Sections 5.0 and 7.0, the capability to achieve 20% onboard wavelength calibration is fully verified.

Item K - Exposure Intervals: This capability was fully verified during the calibration tests (among others) undertaken to obtain the results given in Sections 3.3.2 and 3.3.3.

Item L - Instrument Stability and Repeatability: The results of Sections 6.0 and 7.0 indicate that, following the modifications to improve the filter-grating wheel performance and to compensate for its effects, the requirements in Item L can generally be met. One exception, discussed in Section 7.1, is that the performance cannot generally be met when using the smallest aperture within about 4 hours following a HOLD to OPERATE transition or within about 30 minutes (cf. Item N below) following switching detectors on the FOS. These deficiencies are noted in the FOS Users' Notebook prepared by the STScI, and the 4-hour constraint has been incorporated into the FOS Operations Limitations Document.

Item M - Pulse Saturation Error Correction: The results obtained in Section 6.4 allow these corrections to be made to the specified accuracies.

Item N - System Switching Time: The results shown in Section 7.1 verify that this requirement is met. Note that the longer warmup time for the 0.1 arcsecond aperture is shown to be necessary and represents a constraint on the use of the FOS.

Item O - Acquisition: Initially, the results of Section 7.2 proved that this requirement could <u>not</u> be met. However, with the modifications made to improve the filter-grating wheel performance, to add the LEDs, and to modify the target acquisition algorithms, it is anticipated that this requirement can be met.

Further testing is underway to substantiate this, however. (As a legalistic matter, even the unimproved instrument might have been able to have met this requirement, but not in any matter which would be of practical efficiency for on-orbit observations. The observer would have spent nearly all the precious HST time trying to acquire the target rather than obtaining spectra.)

Item R - Derived Limiting Magnitude: Although this specification is given for informational purposes only (it is simply derivable from other specifications), it is of interest to note that the FOS should exceed a signal-to-noise ratio of at least 6 in each pixel at resolution around 1200 when observing a magnitude 23 unreddened AO pointlike source.

Item S - Mechanism Uncompensated Momentum: The calibrations discussed in this report did not address this item. (However, the FOS filter-grating wheel was redesigned in order to meet this requirement.)

3.0 FOS DESIGN AND FUNCTION

3.1 Description of Instrument

The Faint Object Spectrograph (FOS) is a dual optical channel spectrograph in a near Wadsworth configuration, operating with two independent 512 element linear array pulse-counting digicons. The FOS is designed to achieve high signal-to-noise ratios on very faint astrophysical sources at moderate to low spectral resolving powers. Thus, a premium has been placed on high throughput at ultraviolet and visible wavelengths, on high detector quantum efficiencies, and on lower internal noise in its design. Emphasis has also been given to providing high spatial resolution so that the FOS can isolate fine angular structure in a variety of source geometries. This has led to the provision of twelve selectable entrance apertures of various sizes and shapes, and to packaging of the optical train so that these apertures are located as closely as possible to the telescope's optical axis to minimize optical aberrations. High photometric accuracy has been provided by the detectors which are linear over a wide dynamic range, by the design of precision mechanisms for repeatability and by stable structures with very tight tolerances. Finally, the FOS has been designed for scientific versatility by including provisions for ultraviolet spectropolarimetric measurements, and for high time resolution (10 ms) spectroscopic observations of rapidly varying sources.

The FOS will function as an element of the Space Telescope system, and as such, it is dependent upon the ST for environmen-

tal protection, structural support, electrical power, data management, and communications. The FOS optical system is specifically designed to accept the light beam provided by the ST Optical Telescope Assembly (OTA) as acquired using ST Guidance and Stabilization. The functional design of the FOS (illustrated in Figure 3.1-1) is notable for its simplicity and compact geometry. The observer may select, by orientation of the spacecraft, either of two independent optical channels, each of which focuses nearly stigmatic spectral images on the photocathodes of photon-counting Digicon detectors. These optical channels differ only in the wavelength sensitivity of their respective detectors.

A light beam from the OTA enters the FOS through an entrance port (see Figure 3.1-2). The entrance port provides a light-tight door to close the system when it is not in use. At the focal plane of the f/24 ST input beam is an aperture wheel containing two sets of 12 apertures (see Table 3.1-1) from which a required aperture can be selected to use in each of two optical paths. Each optical beam may be passed through a polarization analyzer, or this device may be rotated out of the beam. The polarization analyzer consists of a magnesium fluoride wave-plate, which is rotated in steps of 22.5 degrees, and a magnesium fluoride Wollaston prism.

The deflection mirror, a "roof" prism, then reflects the beam 22 degrees upward towards the gratings detectors. This simple design feature has the important effect of allowing the apertures to be placed within 61 mm of the telescope optical

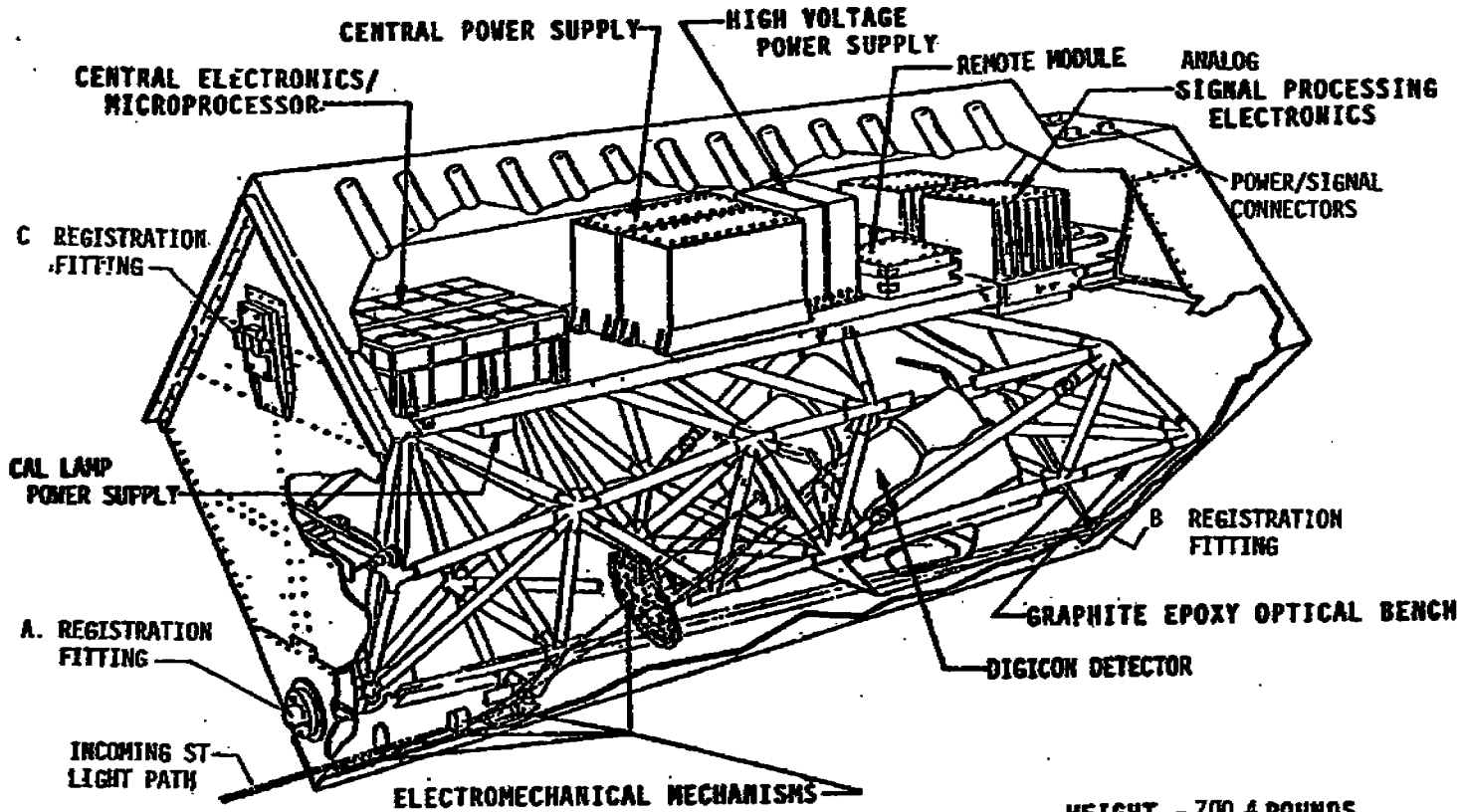
CENTRAL POWER SUPPLY
HIGH VOLTAGE POWER SUPPLY
REMOTE MODULE
ANALOG SIGNAL PROCESSING ELECTRONICS
CENTRAL ELECTRONICS/ MICROPROCESSOR
POWER/SIGNAL CONNECTORS
C REGISTRATION FITTING
CAL LAMP POWER SUPPLY
B REGISTRATION FITTING
GRAPHITE EPOXY OPTICAL BENCH
A. REGISTRATION FITTING
DIGICON DETECTOR
INCOMING ST LIGHT PATH
ELECTROMECHANICAL MECHANISMS
ENTRANCE PORT
ENTRANCE APERTURE
POLARIZER
FILTER/GRATING WHEEL
WEIGHT - 700.4 POUNDS
SIZE - 86.6" x 35.4"
POWER - 135 WATTS

FIGURE 3.1-1

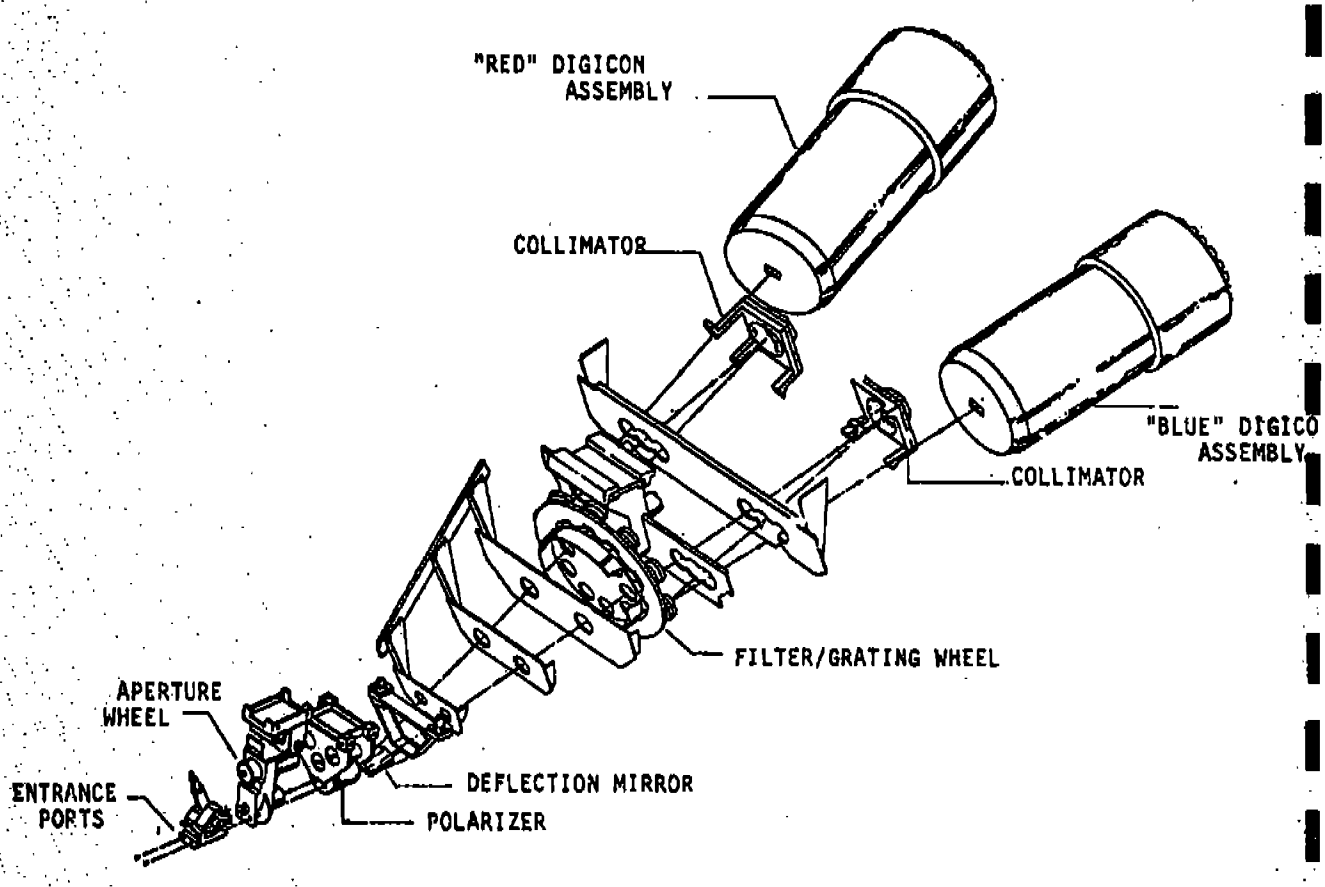

Figure 3.1-2. Optical Ray Trace

TABLE 3.1-1

PRIMARY ENTRANCE APERTURES

Number	Shape	Size* (arcsec)	Center-to-Center Separation (arcsec)	Special Purpose
Single	Round	0.5 dia	N/A	Polarimetry
Single	Round	0.3 dia	N/A	Polarimetry
Single	Round	1.0 dia	N/A	Polarimetry
Blank	N/A	N/A	N/A	Light Shield
Single	Square	4.3	N/A	Target Acquisition
Pair	Square	0.5	3.0	Object and Sky
Pair	Square	0.25	3.0	Object and Sky
Pair	Square	0.1	3.0	Object and Sky
Pair	Square	1.0	3.0	Object and Sky
Single	Rectangular	0.25 x 2.0	N/A	Extended Objects
Single	Square	2.0	N/A	Surrounding Nebulosity
Single	Rectangular**	0.7 x 2.0	N/A	Surrounding Nebulosity

FAILSAFE ENTRANCE APERTURE

Pair	Square	0.5 & 4.3	4.4	Target Acquisition and Spectroscopy

*For rectangular apertures, first dimension is along dispersion, second perpendicular to dispersion.

**With occulter bar which is 0.9 arcsec wide in cross-dispersion direction.

axis, physically close to a corner of the instrument, to minimize astigmatism, while also allowing the bulkier components of the spectrograph to be compactly packaged. The reflected beam then passes through an order-sorting filter, if required, in the filter-grating wheel. It is then collimated by an off-axis paraboloidal mirror and then dispersed and focused by the selected element of the filter-grating wheel onto the detector photocathodes. The dispersing elements on the filter-grating wheel allow FOS to operate at either of two resolutions, moderate ($R = \lambda/\Delta\lambda = 1230 \pm 165$) or lower ($R = 195 \pm 165$). For moderate resolution observations, the dispersing elements are concave gratings which focus first-order spectra onto the detector photocathodes. In this mode, the wavelength range 1150 Å to 8500 Å is divided into six overlapping intervals (see Table 3.1-2), covered by six suitably blazed gratings with ruling frequencies ranging from 168 to 954 lines/mm. Resolution elements vary in width from 1.1 Å in the far ultraviolet to 6.0 Å at red wavelengths. At low dispersion, concave gratings, with ruling frequencies of 144 and 40 lines/mm, are used for wavelength intervals 1150 Å to 2200 Å and 4000 Å to 8000 Å, respectively, giving corresponding resolution elements of 6.9 Å and 25 Å. At intermediate wavelengths, 2600 Å to 7000 Å, low dispersion spectra are obtained with the combination of a double-pass, small-angle sapphire prism and a concave mirror, mounted in the filter-grating wheel. The nonlinear dispersion of this element results in resolution varying from 7.4 Å in the ultraviolet to 350 Å in the red. In return for the reduced spectral resolution, the low dispersion prism

TABLE 3.1-2

WAVELENGTH COVERAGE OF FOS

Element	Resolution at Central Wavelength ($R = \lambda/\Delta\lambda$)	Dispersers	Wavelength (nm) Min	Max
Grating H13	1200		110	164
Grating H19	1200		153	228
Grating H27	1200		221	329
Grating H40	1200		319	474
Grating H57	1200		459	683
Grating H78	1200		626	931
Grating L16	200		110	220
Prism	100		250*	700**
Grating L60	200		400	800
Mirror	1		110	900

Blocking Filters

Element	Wavelengths (nm) T = 1%	T = 90%	Minimum Wavelength (nm) Mode	Transmission at Min. Wavelength
FH27 = fused silica	>165	<200	221	93%
FH40 = WG 305	290	340	319	87%
FH57 = GG375 G34	355	425	459	91%
FH78 = OG 530	510	550	626	91%
FL60 = CG375 G34	355	425	400	85%

*Resolution is about 400 at 250 nm

**Resolution is about 25 at 700 nm

provides excellent throughput and image quality, emphasizing spectrophotometry of the very faintest sources to be observed with the FOS. Wavelength calibration is provided by two on board PtCrNe lamps (Figure 3.1-3). The two Digicon detector assemblies, designated "red" and "blue", differ only in their photocathode and face-plate materials (Figure 3.1-4). The "blue" detector has a bialkali photocathode (NaKSb), which is most sensitive at blue and ultraviolet wavelengths, deposited on a magnesium fluoride window. The photocathode of the "red" detector, trialkali NaKSb(Cs) deposited on fused silica, provides an extension of sensitivity to the red, at the expense of higher thermionic noise at ambient temperatures. To reduce background to the extremely low values (< 0.002 counts/s/diode) required for the FOS scientific programs, both photocathodes are cooled (Figure 3.1-5) to the temperature range $-10^{o}C$ to $-28^{o}C$. The Digicon detector assemblies operate by focusing photoelectrons emitted by the photocathode, and accelerated through a potential difference 22.5 KeV, onto a linear array of 512 silicon diodes (see Figures 3.1-6 and 3.1-7). Focusing is accomplished with a SmCo permanent magnet assembly, carefully shaped to provide extremely uniform fields. The electron beam can be deflected parallel or perpendicular to the diode array, so that images from any part of the cathode may be centered on the linear array. This facilitates comparison of sky background and source images and is required for polarimetric observations. The size of each diode, 40 microns by 200 microns, is the optimum to minimize dark noise, while still being large enough to prevent a signifi-

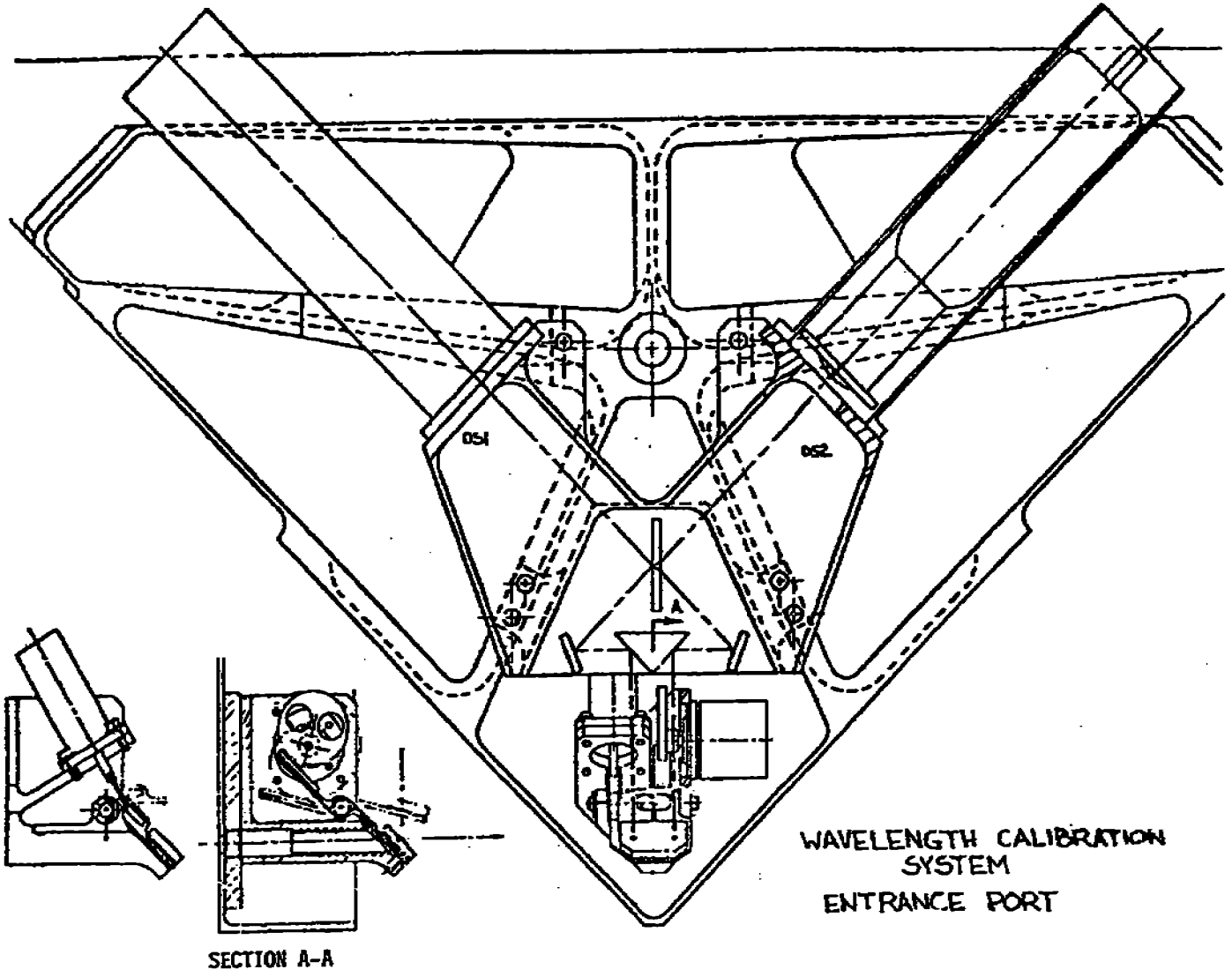
OS1
OS2
A
A
SECTION A-A
WAVELENGTH CALIBRATION
SYSTEM
ENTRANCE PORT

FIGURE 3.1-3

Flight Tube Quantum Efficiency

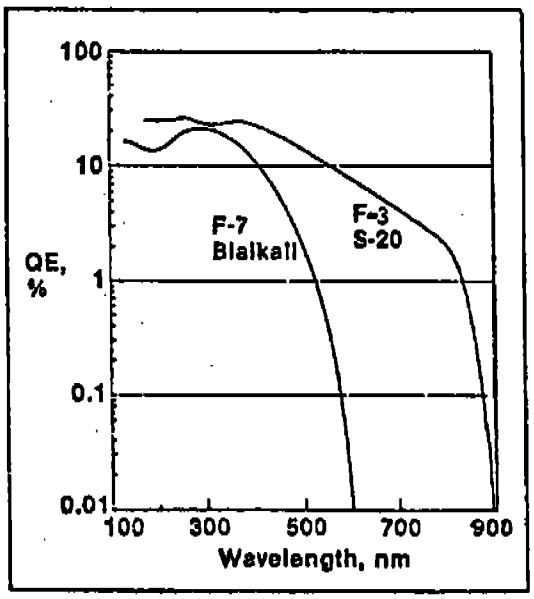

Figure 3.1-4. Detector Quantum Efficiencies (Quantum efficiencies of the two FOS flight detectors. Both produce under 0.002 counts/diode/sec noise at -10°C.

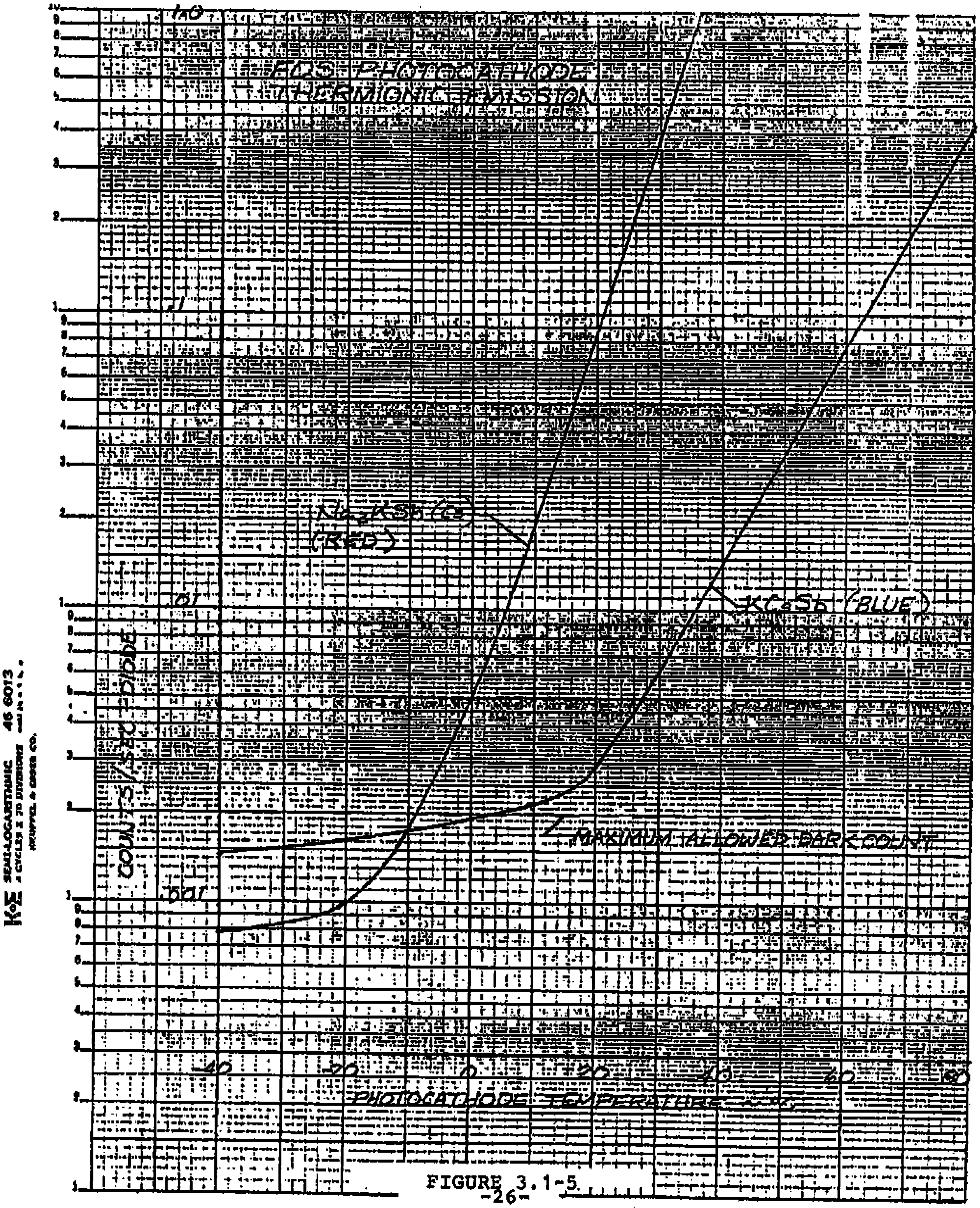
FOS PHOTOCATHODE
THERMIONIC EMISSION
COUNTS/SEC/DIODE
10
1
.1
.01
.001
Na2KSb (Cs)
(RED)
KCsSb (BLUE)
MAXIMUM ALLOWED DARK COUNT
-40
-20
0
20
40
60
80
PHOTOCATHODE TEMPERATURE
K&E SEMI-LOGARITHMIC 46 6013
3 CYCLES X 70 DIVISIONS
KEUFFEL & ESSER CO.

FIGURE 3.1-5

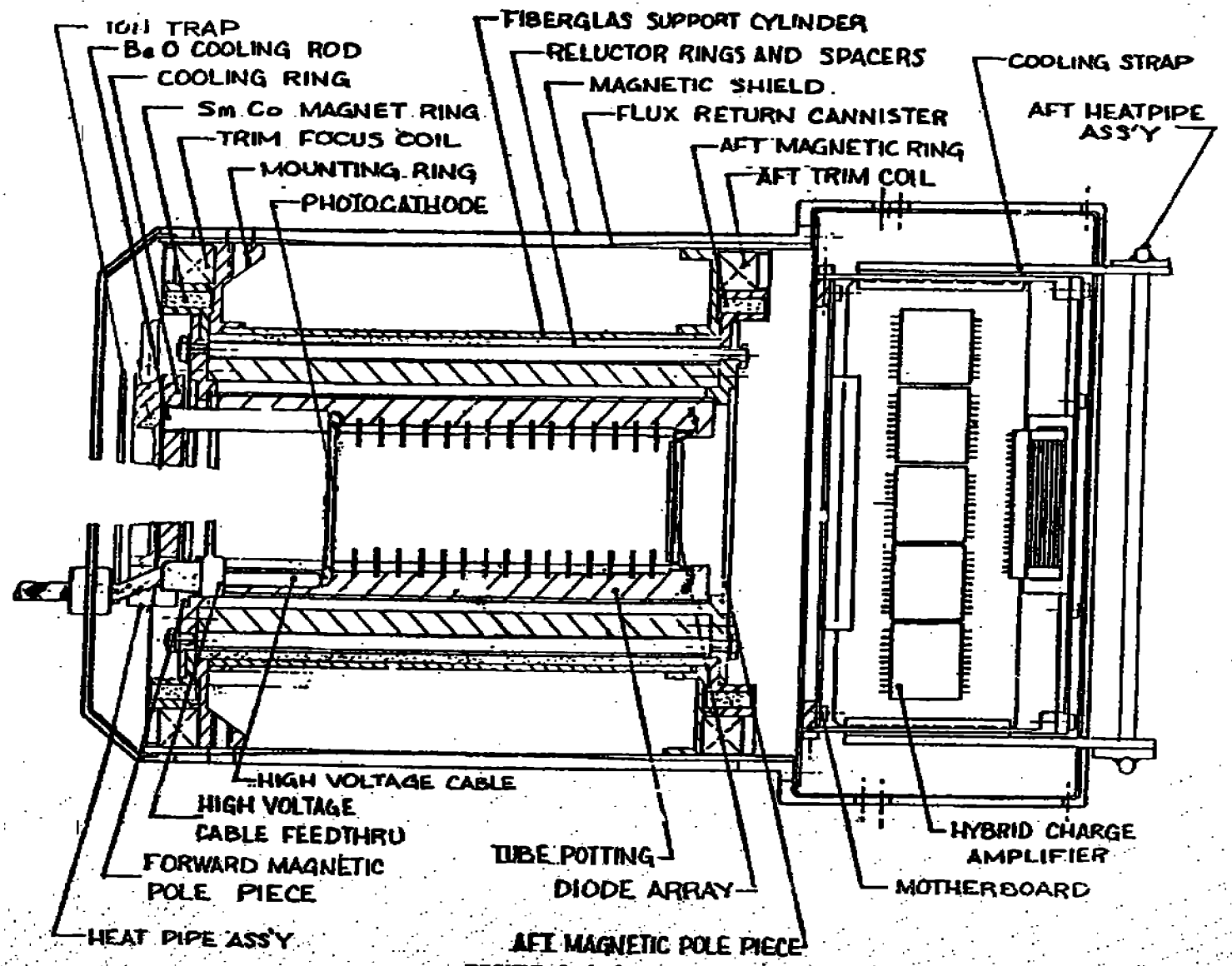
ION TRAP
BeO COOLING ROD
COOLING RING
Sm Co MAGNET RING
TRIM FOCUS COIL
MOUNTING RING
PHOTOCATHODE
FIBERGLAS SUPPORT CYLINDER
RELUCTOR RINGS AND SPACERS
MAGNETIC SHIELD
FLUX RETURN CANNISTER
AFT MAGNETIC RING
AFT TRIM COIL
COOLING STRAP
AFT HEATPIPE ASS'Y
HIGH VOLTAGE CABLE
HIGH VOLTAGE CABLE FEEDTHRU
FORWARD MAGNETIC POLE PIECE
TUBE POTTING
DIODE ARRAY
HYBRID CHARGE AMPLIFIER
MOTHERBOARD
HEAT PIPE ASS'Y
AFT MAGNETIC POLE PIECE

FIGURE 3.1-6

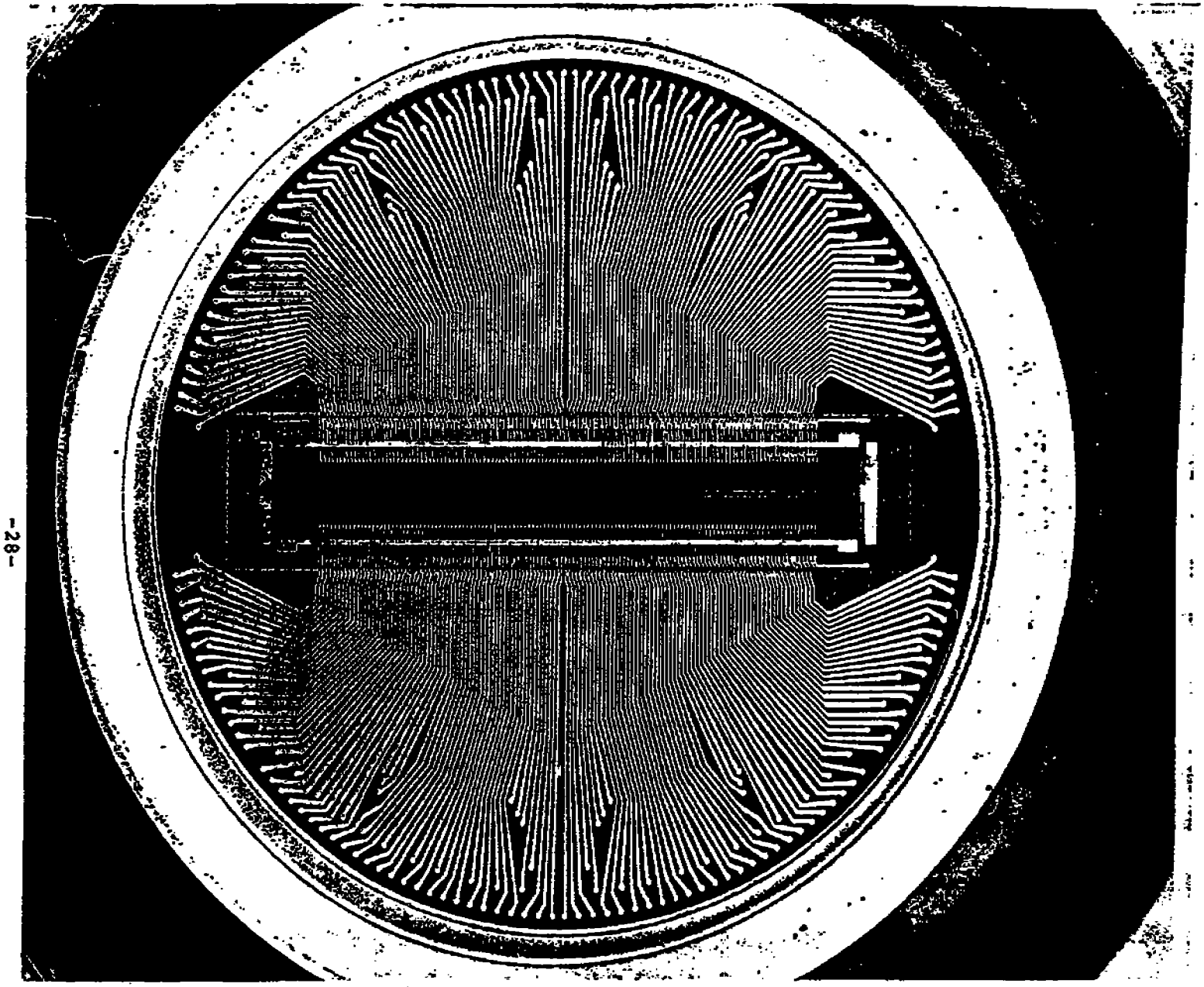

FIGURE 3.1-7

cant loss of signal at the diode ends. The charge pulse generated in each diode is amplified and counted by one of 512 independent electronic chains. The electronics amplify the charge generated on each diode and process the data for transmission to the SI Command and Data Handling (C&DH) system. The electronics also provide operations control of all FOS subsystems (see Block Diagram Figure 3.1-8). FOS power supplies condition SSM power and provide required low voltage to the other electronics and high voltage to the detectors and calibration lamps as needed. The optics and detectors are mounted on an optical bench structure which maintains extremely fine dimensional stability. In order to maintain dimensional stability under varying thermal conditions, the bench structure is made of graphite epoxy tubes and invar joints. The bench is connected to the FOS shell structure using a nonredundant support which prevents structural loads in the interfacing structure from inducing stress deformations into the optical bench. The optical elements are moved into very precise positions in the optical path by mechanisms which are mounted on an optical bench (Figure 3.1-9). The grating wheel is stepper-motor driven and uses a spring-loaded cam follower and machined detents. The others use encoded stepper motors to achieve accurate positional repeatability. All mechanisms have fail-safe or redundant devices which will avoid debilitating single-point failures.

To obtain the required detector dark count, the photocathode of the detectors must be cooled. The detectors are passively cooled by heat pipes connected from the photocathode and charge

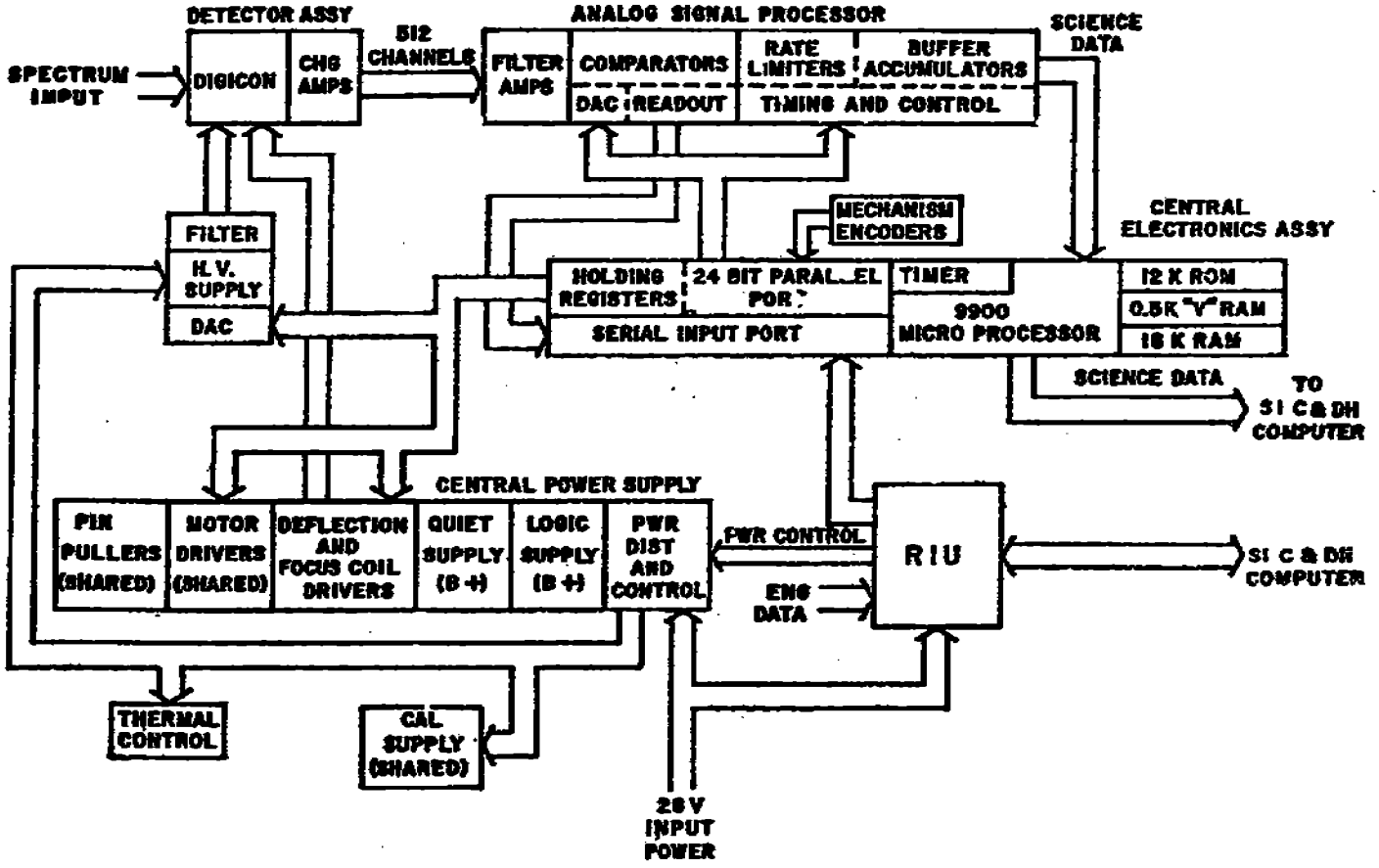

Figure 3.1-8. FOS Electrical Block Diagram

MECHANISMS LOCATIONS

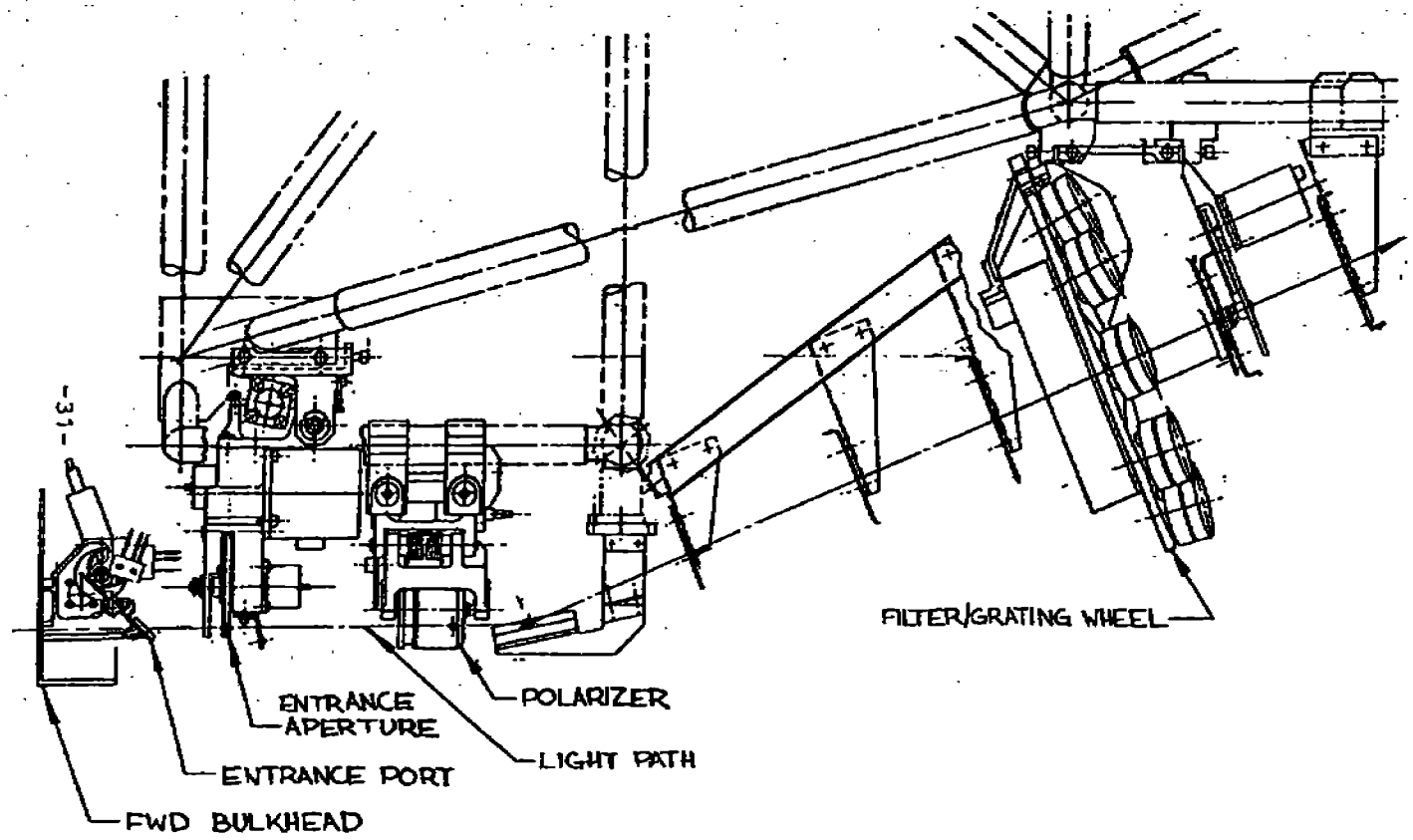

FIGURE 3.1-9

amplifiers to two dedicated radiators, one for the photocathodes and one for the charge amplifiers. Also, precise thermal control is required for dimensional stability of the optical bench. The thermal control system consists of sensors, control circuitry, heaters, heat pipes, radiators, thermal isolators and insulation. The optics compartment temperature is maintained by six heaters powered by either electronics string. The system is controlled by selective use of heaters, radiators, and insulation (Figure 3.1-10).

Electrical and mechanical Ground Support Equipment (GSE) are used to operate, manipulate, handle, and store the FOS (Figures 3.1-11 and 3.1-12).

The structural enclosure of the FOS (Figure 3.1-13) is made of aluminum honeycomb skin and stringer construction. The dedicated radiators transfer internally generated heat to the SSM aft shroud heat sinks. Externally, there are also hand holds for use by the astronaut and attachment points for ground handling. Guide rails provide orientation for installation into and removal from the focal plane structure. Electrical connectors which can be mated and demated in-orbit are also provided. A vent with filter allows for pressure equalization during ground transportation, ascent and re-entry. An ion gauge permits evaluation of on-board pressure.

The FOS is designed to fit in axial ST Positions Two or Four and is assigned to Position Two. A three-point attachment latching mechanism holds the instrument in place and provides registration of the FOS apertures where the f/24 beam of the OTA

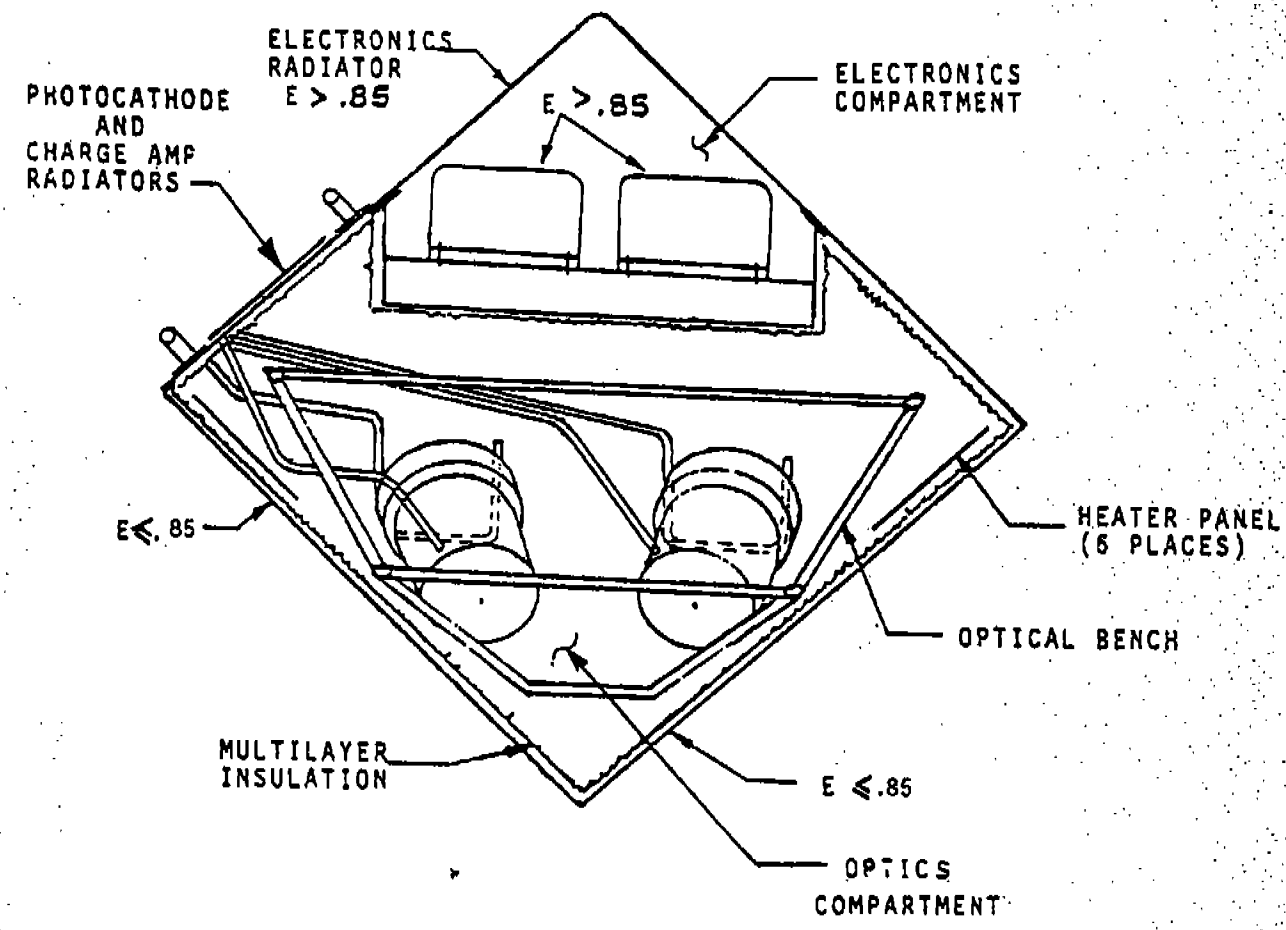

Figure 3.1-10. Thermal Control Subsystem

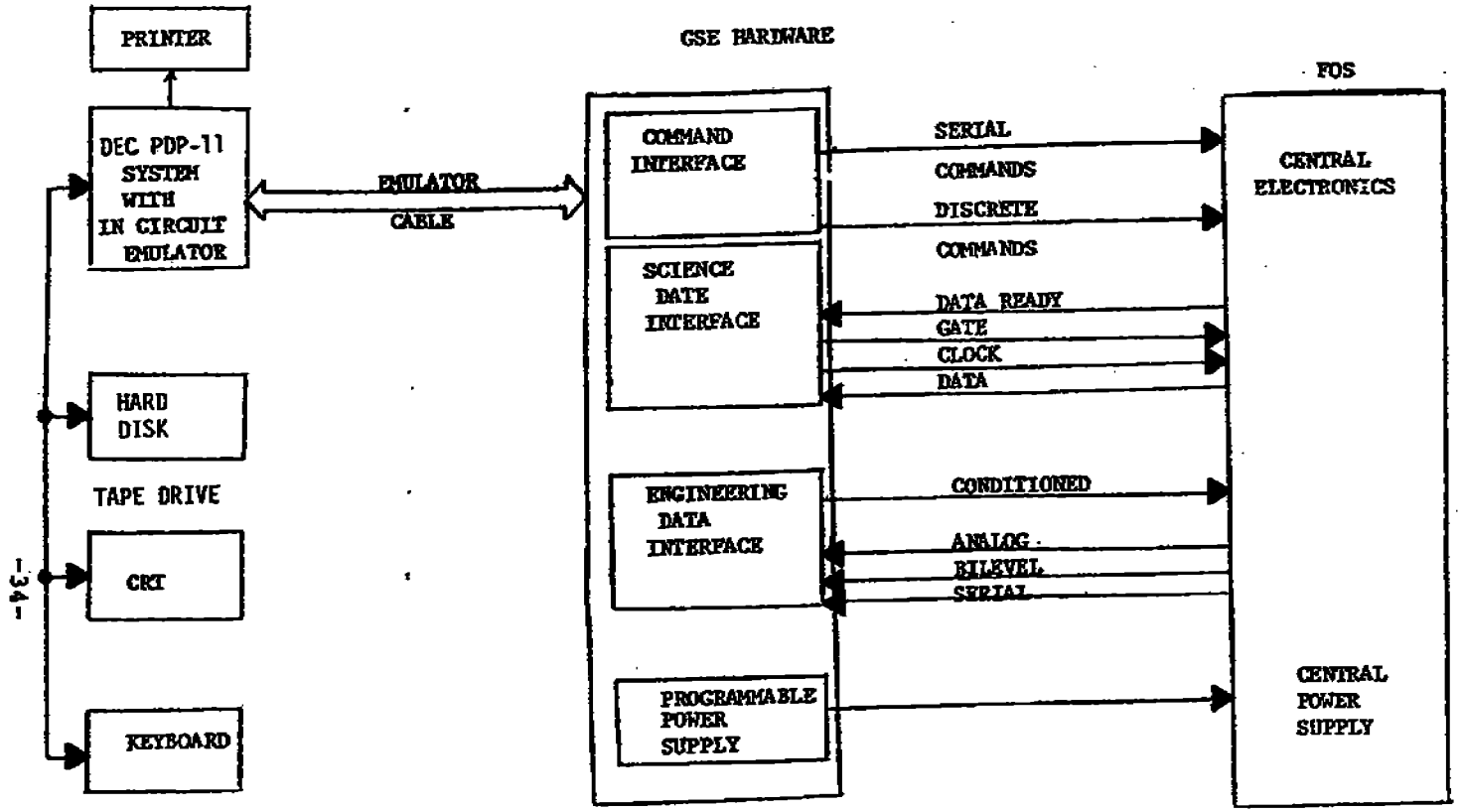

Figure 3-1-11. GSE Block Diagram

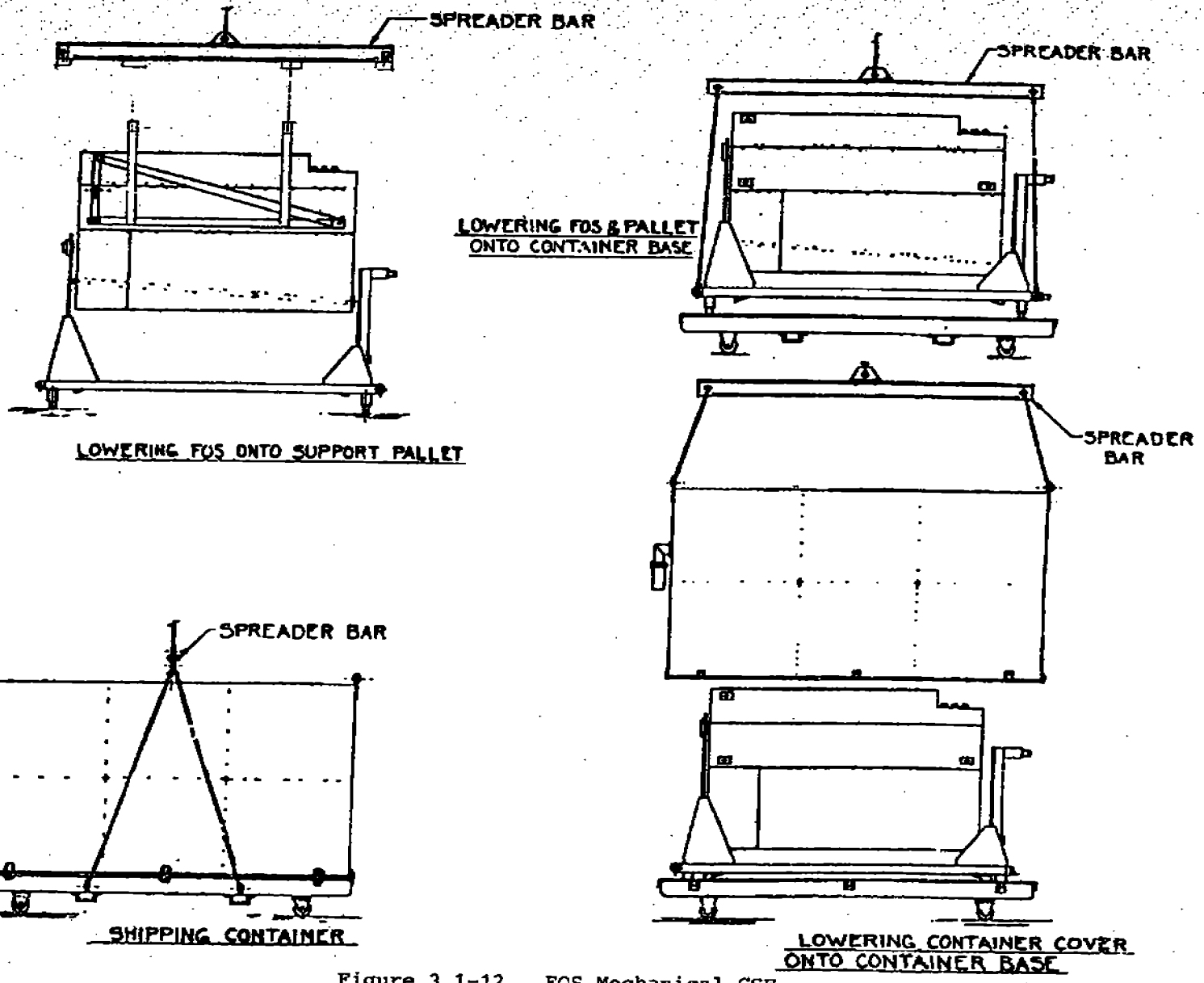

Figure 3.1-12. FOS Mechanical GSE

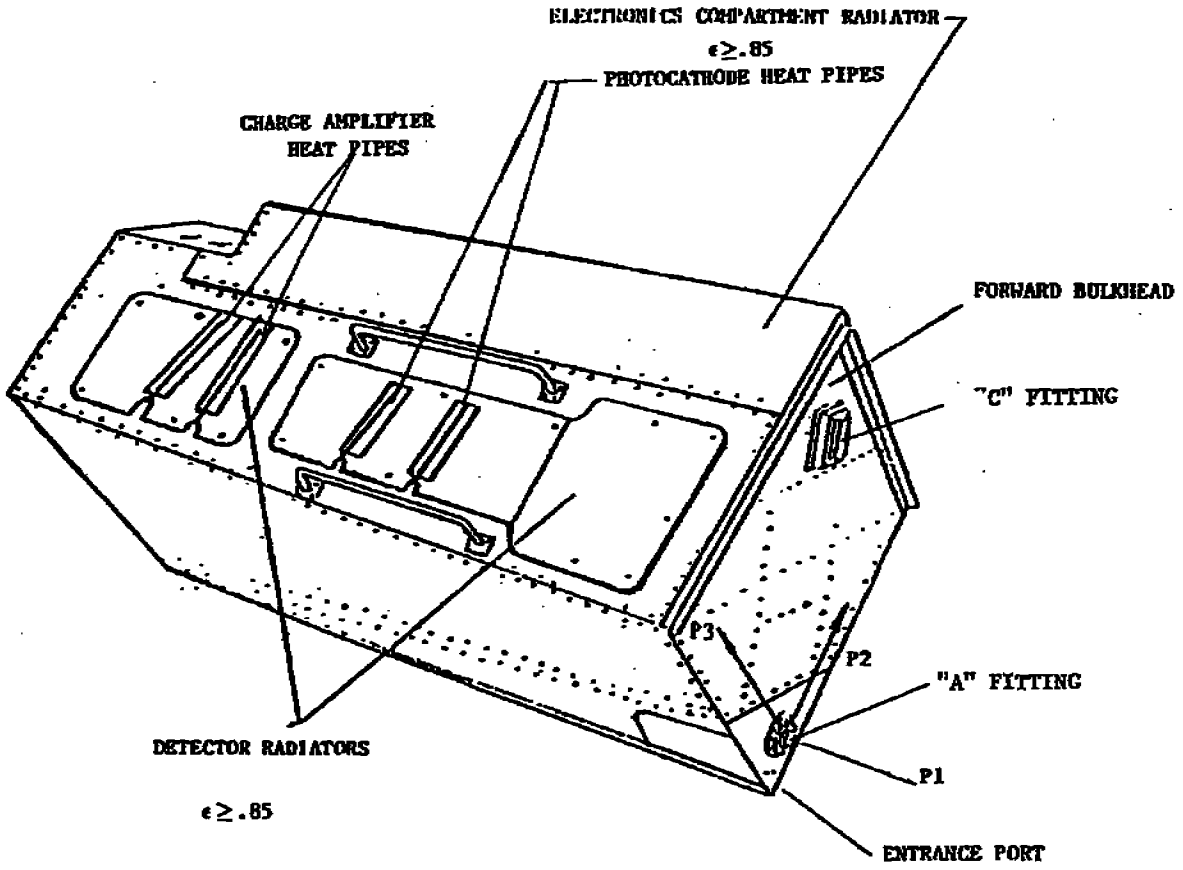
ELECTRONICS COMPARTMENT RADIATOR
ε≥.85
PHOTOCATHODE HEAT PIPES
CHARGE AMPLIFIER
HEAT PIPES
FORWARD BULKHEAD
"C" FITTING
P3
P2
"A" FITTING
P1
ENTRANCE PORT
DETECTOR RADIATORS
ε≥.85

FIGURE 3.1-13

comes to a focus.

In summary, Figure 3.1-1 illustrates the FOS overall design concept and identifies the major assemblies of the instrument summarized in Table 3.1-3. Figure 3.1-14 defines the FOS/ST interfaces.

3.2 Set-Up Parameters

3.2.1 High Voltage and Trim Focus

3.2.1.1 Digicon Focus Condition - The digicon sensor is a magnetically focused image tube with optimum electromagnetic focus when

$$B = kV \quad ,$$

where B is the focus magnetic field
V is the tube voltage
k is a constant

The main focus magnetic field is generated by a permanent magnet focus assembly (PMFA). In addition, a solenoid is wound interior to the PMFA. By utilizing this trim focus field, the digicon tube remains in electromagnetic focus from the maximum allowable 24 kilovolts down to approximately 18 kilovolts. This option was deemed prudent in the unlikely event of a high voltage discharge; the voltage could then be reduced down to 18 kilovolts to eliminate the discharge.

3.2.1.2 Focus Calibration - Using the spectral calibration, the tube focus condition is determined by finding the minimum spectral line width as a function of high voltage. Note that the unblended spectral line chosen to establish high voltage

TABLE 3.1-3

IDENTIFICATION OF MAJOR COMPONENTS/ASSEMBLIES

	Assemblies	Subassemblies	Key Components
1.	Detector Assembly	Deflection/Trip Focus Coils	Coils/Drivers
		Permanent Magnet Focus Assy	Magnets/Reflector Rings
		Digicon	Headers
			Diode Array
			Seals
			Faceplate
		Charge Amplifier	Hybrids
2.	Optical Bench Assembly	Optical Bench Structure	Stepper Motors
		Aperture Entrance	Encoders/Detents
		Polarizer	Pin Puller
		Filter/Grating Wheel	Heaters
		Optics/Optical Mounts	
3.	Electronics Shelf Assembly	Bench Shelf/Multilayer Insulation (MLI)	
		EMC/EMI Filter	
		High Voltage Power Supply	
		Remote Interface Units (RIUs)/Expander Unit (EU)	
		Expander Unit (EU)	
		Central Power Supplies	
		Analog Signal Processors	
4.	SI Enclosure Assembly	Front/Aft Bulkheads	External Attach Fittings
		Longerons	Entrance Port Mechanism
		Thermal Radiators/Heat Pipes/MLI	Heat Pipes/Interfaces
			Thermal Control Circuits
		Shear Panels	
		Optical Bench Attachment Fittings	
		Calibration Optics	

ID 3611E/AD 0257Q

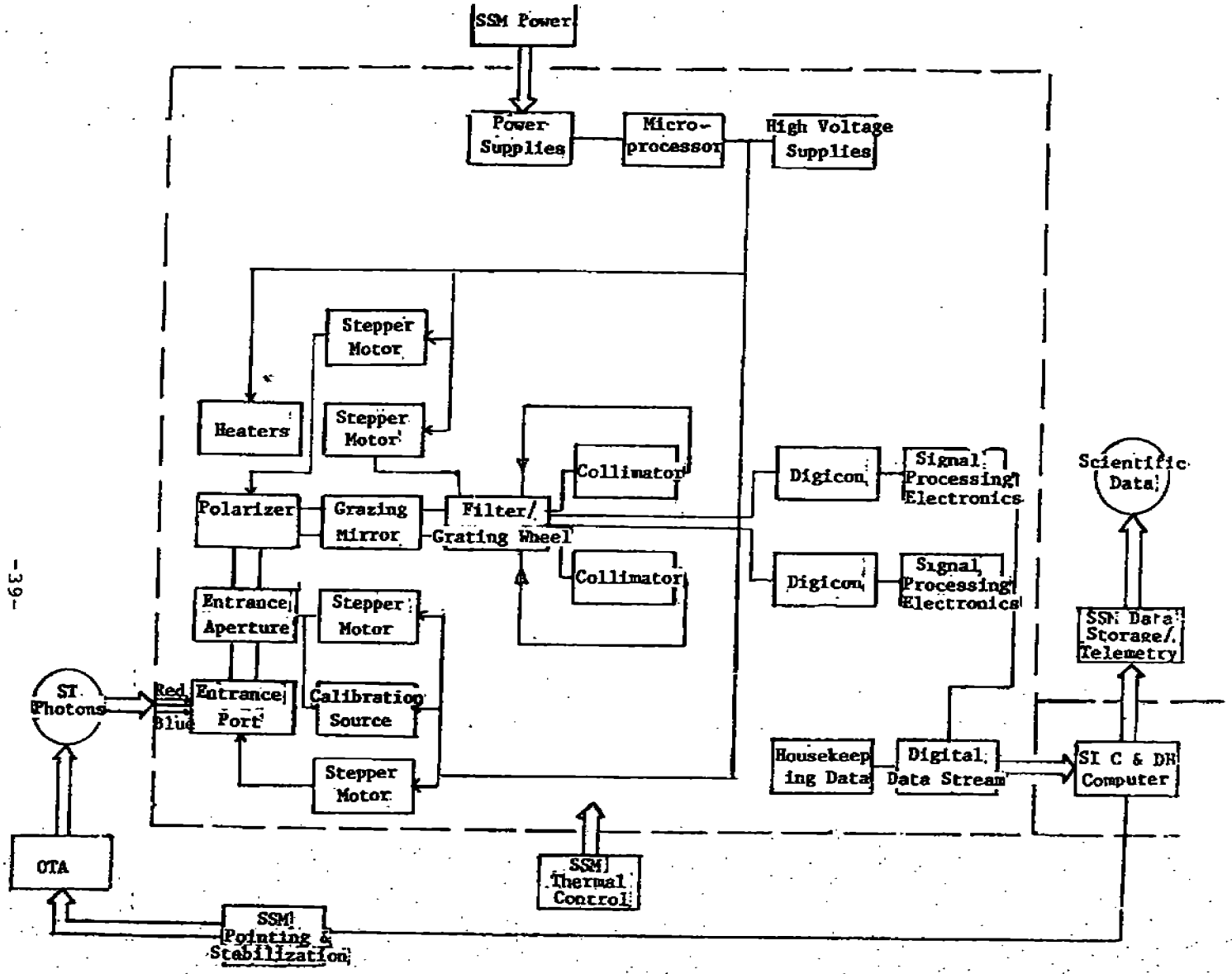

Figure 3.1-14. FOS Interfaces

focus must be near the shortest wavelength accessible by the tube, i.e., about 120 nm for the blue tube and around 200 nm for the red tube. At the shorter wavelengths, the digicon photoelectrons are emitted from the photocathode with relatively high energies and electromagnetic focus requirements are far more severe than at the longer wavelengths.

3.2.1.3 Focus Results - For zero trim focus current Figures 3.2.1-1 through 3.2.1-3 show the red side focus characteristic, spectrum, and focus line, respectively. Similarly for zero trim focus, Figures 3.2.1-4 and 3.2.1-5 show the blue side focus characteristic and focus line, respectively. Focus is excellent at essentially the FOS specification of 1 diode full width half maximum for zero trim focus. For zero trim focus, the red and blue focus voltages are 21.5 and 23.2 kilovolts.

3.2.2 Discrimination Levels

3.2.2.1 Discriminators - Each digicon electronics channel has a separate discriminator circuit. The discriminator allows the low noise counting of single photon events. Channel pulses which are above the discriminator threshold (photon events) are passed onto the counter circuit; whereas channel pulses below the threshold (electronic noise) are rejected. The threshold is set by a digital to analog converter for each channel. The threshold level is variable digitally over a range from 0 to 255. Optimum setting of the discriminator occurs when all electronic noise is rejected and most photon events are counted. On average, this setting is about 180, although each channel is set independently by the technique described next.

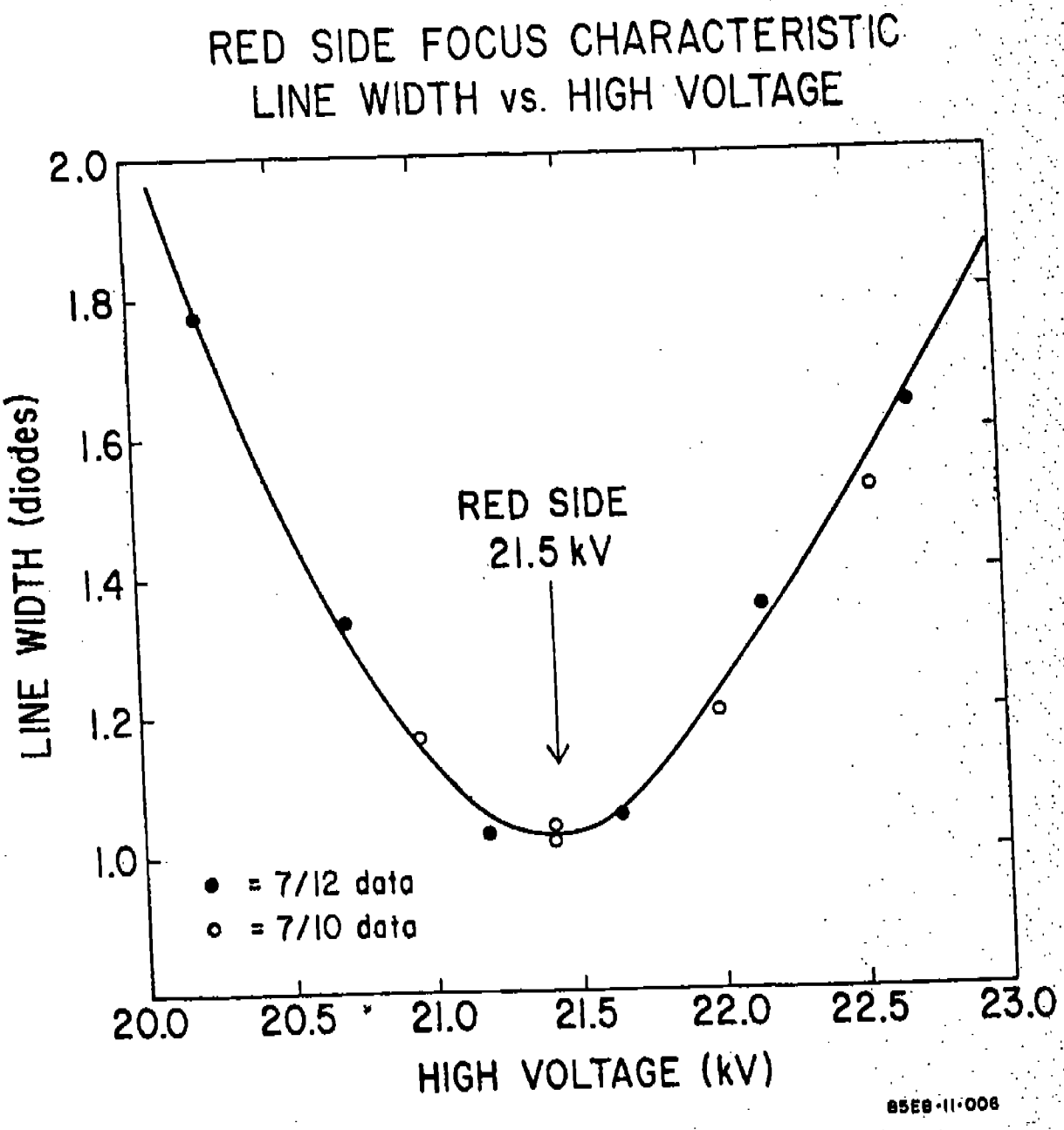
RED SIDE FOCUS CHARACTERISTIC
LINE WIDTH vs. HIGH VOLTAGE
LINE WIDTH (diodes)
2.0
1.8
1.6
1.4
1.2
1.0
RED SIDE
21.5 kV
● = 7/12 data
o = 7/10 data
20.0
20.5
21.0
21.5
22.0
22.5
23.0
HIGH VOLTAGE (kV)
85EB-11-006

FIGURE 3.2.1-1

RED SIDE IN FOCUS SPECTRUM
CENTERED AT 190 NANOMETERS

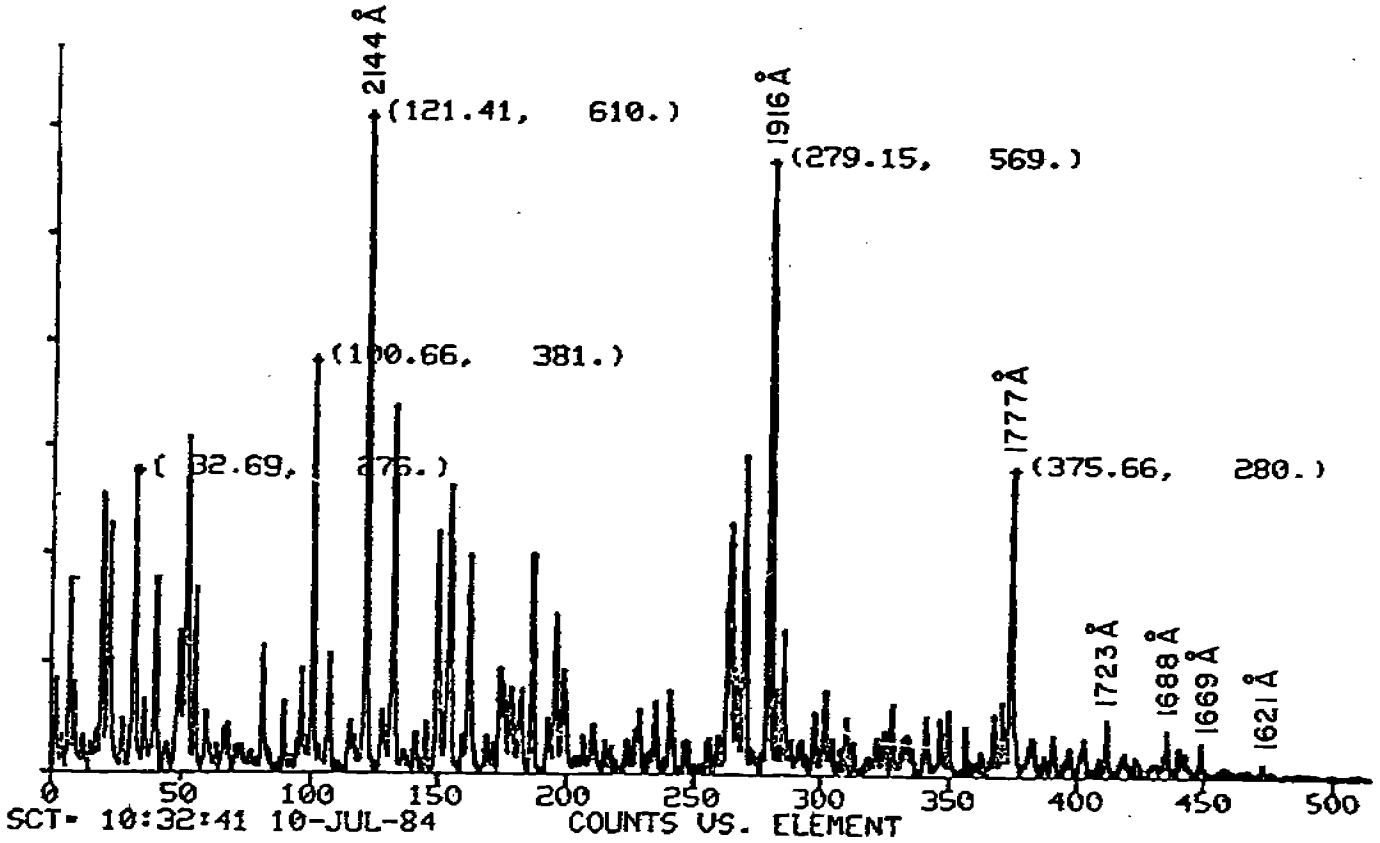

FIGURE 3.2.1-2

85EB-II-014

RED SIDE "IN FOCUS" SPECTRAL
LINE AT 214.4 n.m. (FWHM = 1.04 DIODES)

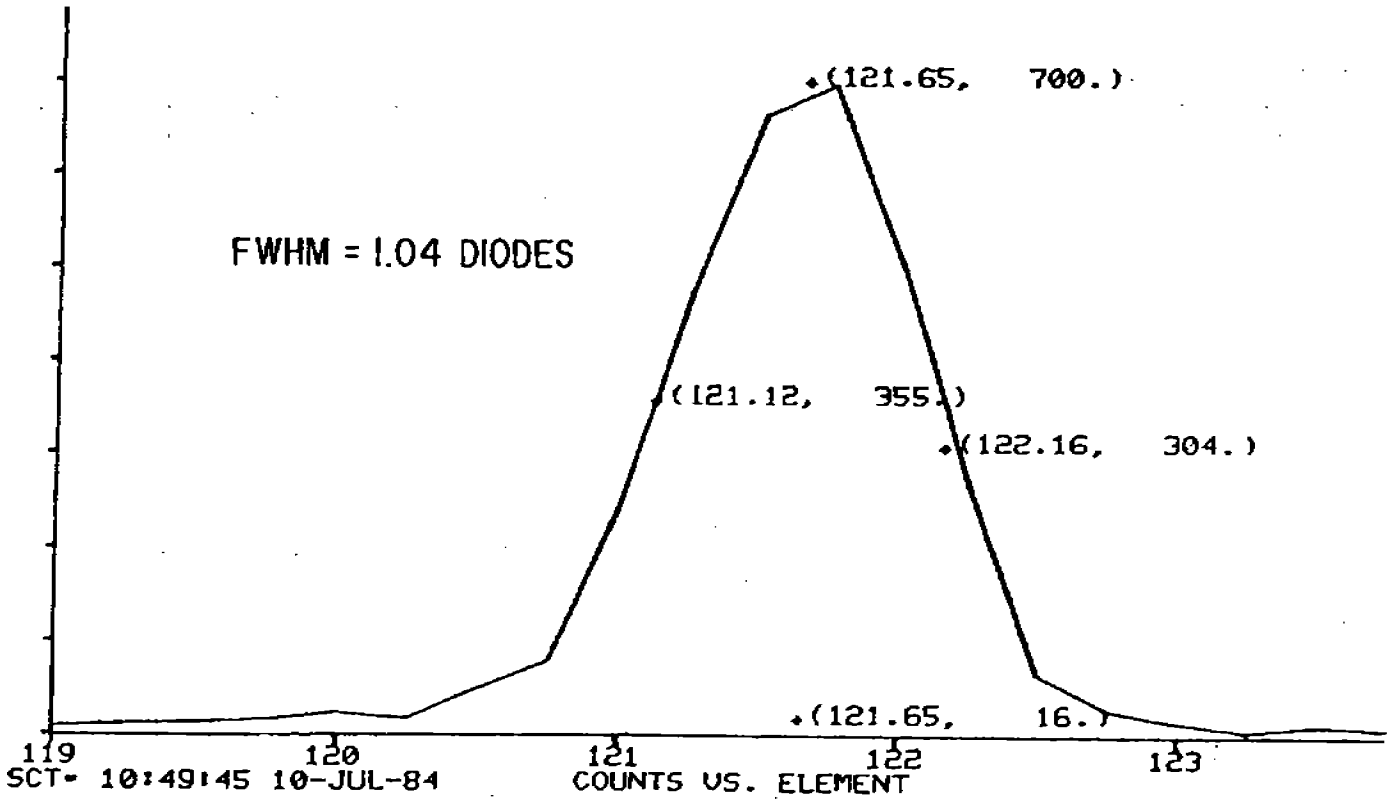

FIGURE 3.2.1-3

85EB-11-008

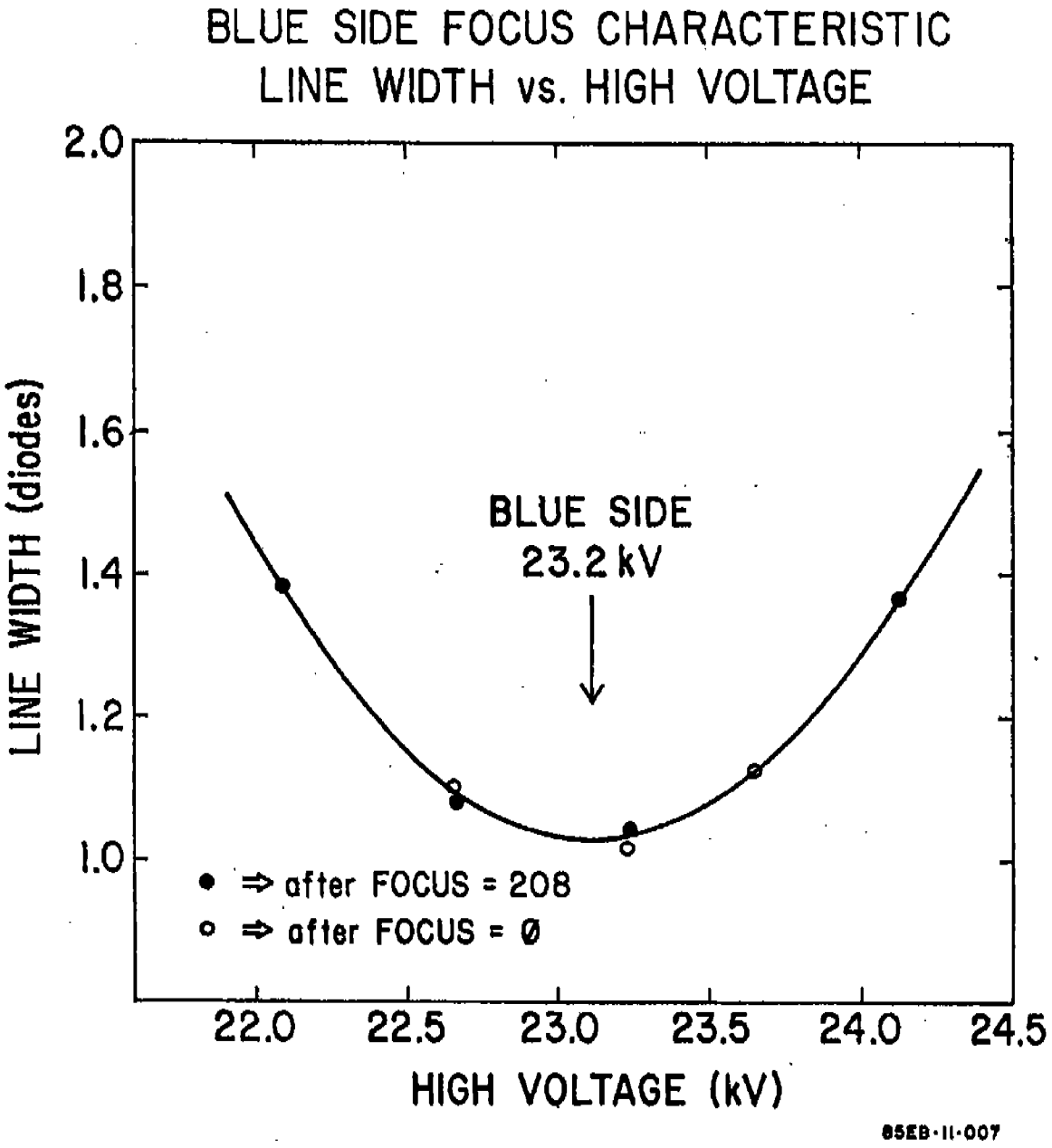
BLUE SIDE FOCUS CHARACTERISTIC
LINE WIDTH vs. HIGH VOLTAGE
LINE WIDTH (diodes)
2.0
1.8
1.6
1.4
1.2
1.0
BLUE SIDE
23.2 kV
● ⇒ after FOCUS = 208
○ ⇒ after FOCUS = Ø
22.0
22.5
23.0
23.5
24.0
24.5
HIGH VOLTAGE (kV)
85EB-11-007

FIGURE 3.2.1-4

BLUE SIDE IN FOCUS
SPECTRA LINE AT ~130 n.m. (FWHM = 1.03 DIODES)

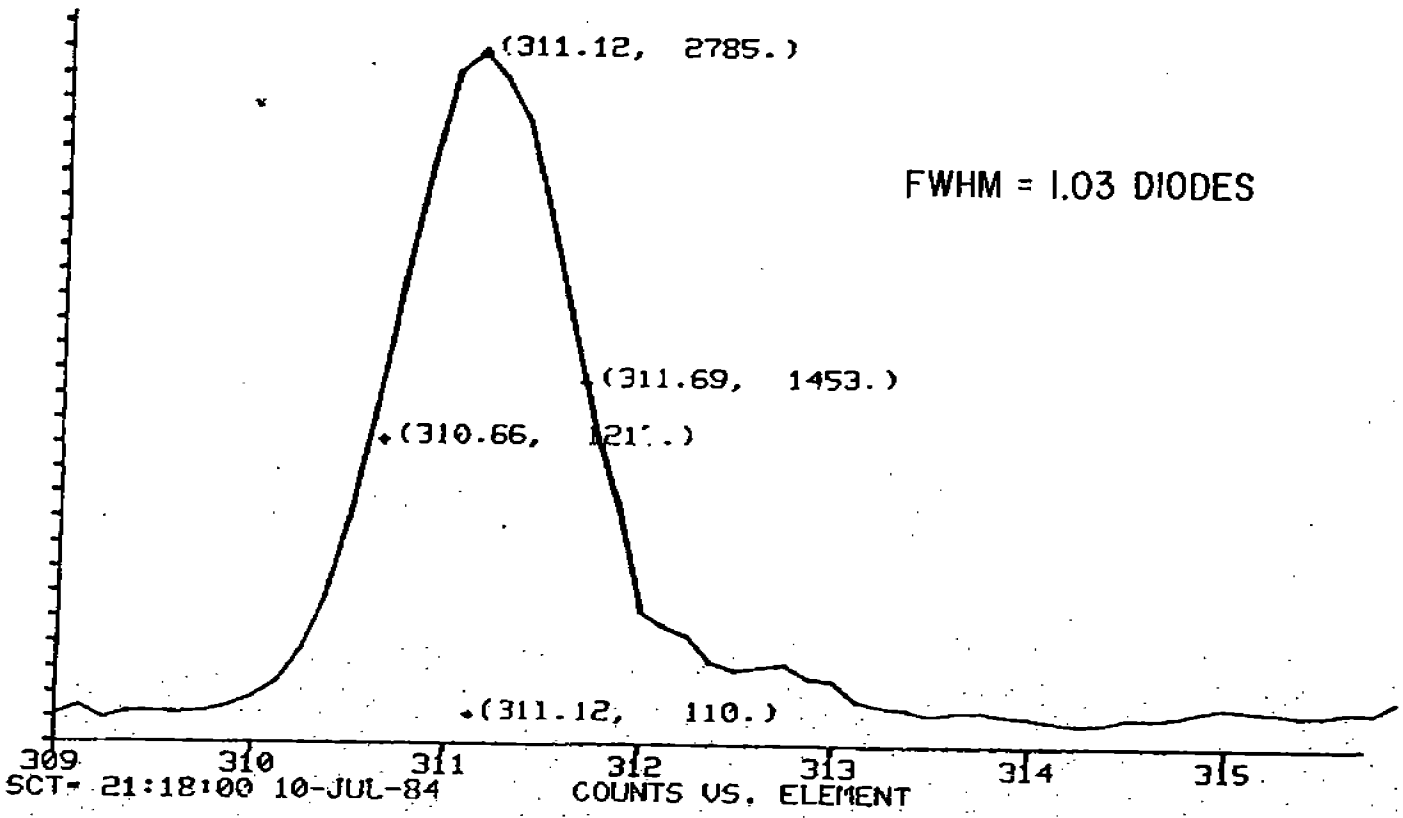

FIGURE 3.2.1-5

85E8-11-009

3.2.2.2 Discriminator Settings - To determine the discriminator settings, the digicon is operated at 12 kilovolts and the discriminators are sequentially incremented to maximum output. In this manner, an integral pulse height distribution is generated for each diode channel. The goal is to set each discriminator at the center of the 12 kilovolt photopeak.

The integral distribution is characterized by a nonlinear distribution at low discriminator settings, a relatively flat mid-level region, and a decreasing nonlinear tail region at high settings. The tail region is the photopeak region. The center of the photopeak discriminator position is given by the discriminator setting which gives one half the count of the flat region.

A value of 12 kilovolts is chosen as the setting for the discriminators to be greater than 3 FWHM above the background noise level for low noise digicon operation. For most channels FWHM $\leq$ 4 kilovolts. The very few channels where FWHM > 4 kilovolts can be (and are) individually disabled.

3.2.2.3 Discriminator Calibration - Standard discriminator settings are automatically loaded from firmware into discriminator registers at instrument turn-on. These settings were determined by the procedure described above. It is anticipated that these settings will be used without major modification for all future data acquisition.

During FOS calibration, we confirmed proper discriminator settings by two techniques: (1) 1000-second background runs; and (2) FOS DAC noise test. For specific results from the background test, refer to Section 6.5 of this Report. In general,

the channel to channel background is determined by photocathode thermionic emission and not electronic noise as should be the case for proper discriminator level settings. However, during the background test, several channels were found to be noisy and will have to be repaired or otherwise disabled by software commands.

DAC noise test calibration results are shown in Figures 3.2.2-1 and 3.2.2.2 for the red and blue side, respectively. In this test, the discriminator threshold is stepped from 0 to 254 so that the integral distribution for each channel is generated. The test is run without light. Anomolous channels are indicated and for the most part are previously identified bad channels.

3.3 Special Function Validation

3.3.1 Hysteresis Mitigation

3.3.1.1 Image Hysteresis - Digicon image acquisition is achieved by stepping current through deflection coils located on the sides of the image tube. Permeable materials located external to this region in the permanent magnet focus assembly introduce counter magnetic fields to the image deflection fields for large deflection steps. This counter magnetic field depends on the previous deflection history. Without a "deperm" procedure, the digicon image position origin would depend on the previous stepping pattern.

3.3.1.2 "Deperm" Procedure - At the beginning of an acquisition during initialization of the setup parameters, the deperm procedure is or is not implemented, depending on the state

```
DAT 04-OCT-84 HTM 12:46:04 MIF= 75 MAF=     0 BSU=2982 BSI= 265 PSS=  11
EHT=SCR    SDT=SCR    SDF=1  PWD=OK HWC=PFU2 PRS=AMB    TMP=RM   SID=A
CMT  FOS_NOISE_VS._DISCRIMINATOR_VALUES_SIDE=A   OPR E. W. STREIN
SNC=  165 WPL=  512 LPF=    2 PLZ=CWOI ENT=  2 FGW=H27 APR=  82 TAX=    0
HOU=    0 LOU=    0 HVD=    0 ARQ=  128 FOC=128 SAF=   0 INM=   0 TAY=    0
XDC=    0 X-P= 1536 X-B=    0 X-S=    1 REF=  5 SLI=   1 MUL=   1 TMX=65535
YDC=    0 Y-P= 2048 Y-B=    0 Y-S=    1 Y-R= 64 CHI=   0 #CH=512 DE1=    0
LIV=  500 DED=  112 NLM=65535 ACM=    8 INT=   1 PTN=   1 RDO=   1 DE2=    0
```

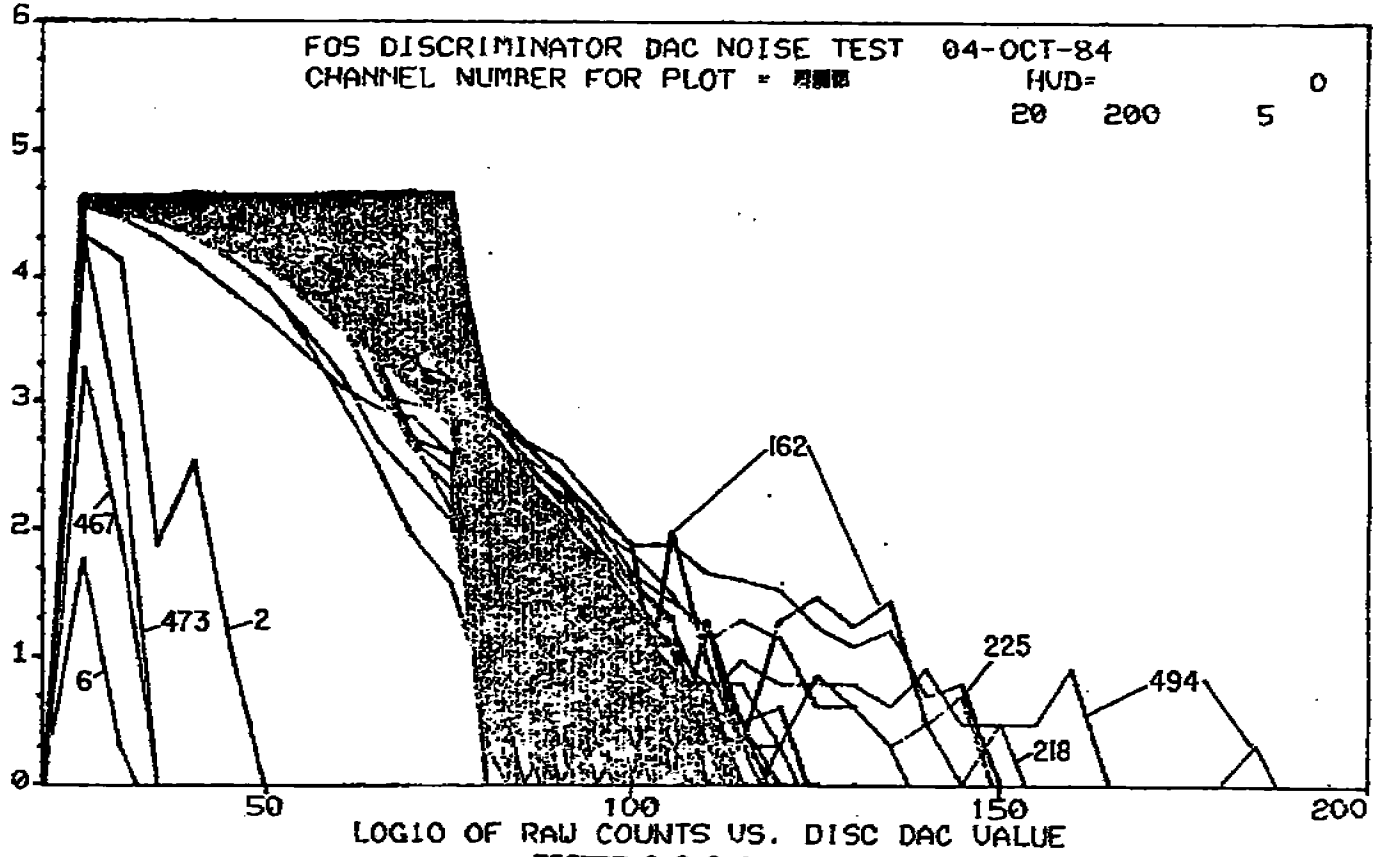

LOG10 OF RAW COUNTS VS. DISC DAC VALUE

FIGURE 3.2.2-1

85EB-11-012

DAT 06-OCT-84 HTM 11:54:30 MIF= 87 MAF= 0 BSV=2975 BSI= 288 PSS= 14
EHT=H003XX SDT=H003XX SDF=1 PWD=OK HWC=PFU2 PRS=AMB TMP=RM SID=B
CMT FOS_NOISE_VS._DISCRIMINATOR_VALUES_SIDE=B OPR E. W. STREIN
SNC= 165 WPL= 512 LPF= 2 PLZ=CW01 ENT= 2 FGW=H40 APR= C2 TAX= 0
HOV= 0 LOV= 1099 HVD= 0 ARQ= 128 FOC=208 SAF= 0 INM= 0 TAY= 0
XDC= 0 X-P= 1536 X-B= 0 X-S= 1 REF= 5 SLI= 1 MUL= 1 TMX=65535
YDC= 534 Y-P= 2048 Y-B= 0 Y-S= 1 Y-R= 64 CHI= 0 #CH=512 DEI= 0
LIV= 500 DED= 112 NLM=65535 ACM= 8 INT= 1 PTN= 1 RDO= 1 DE2= 0

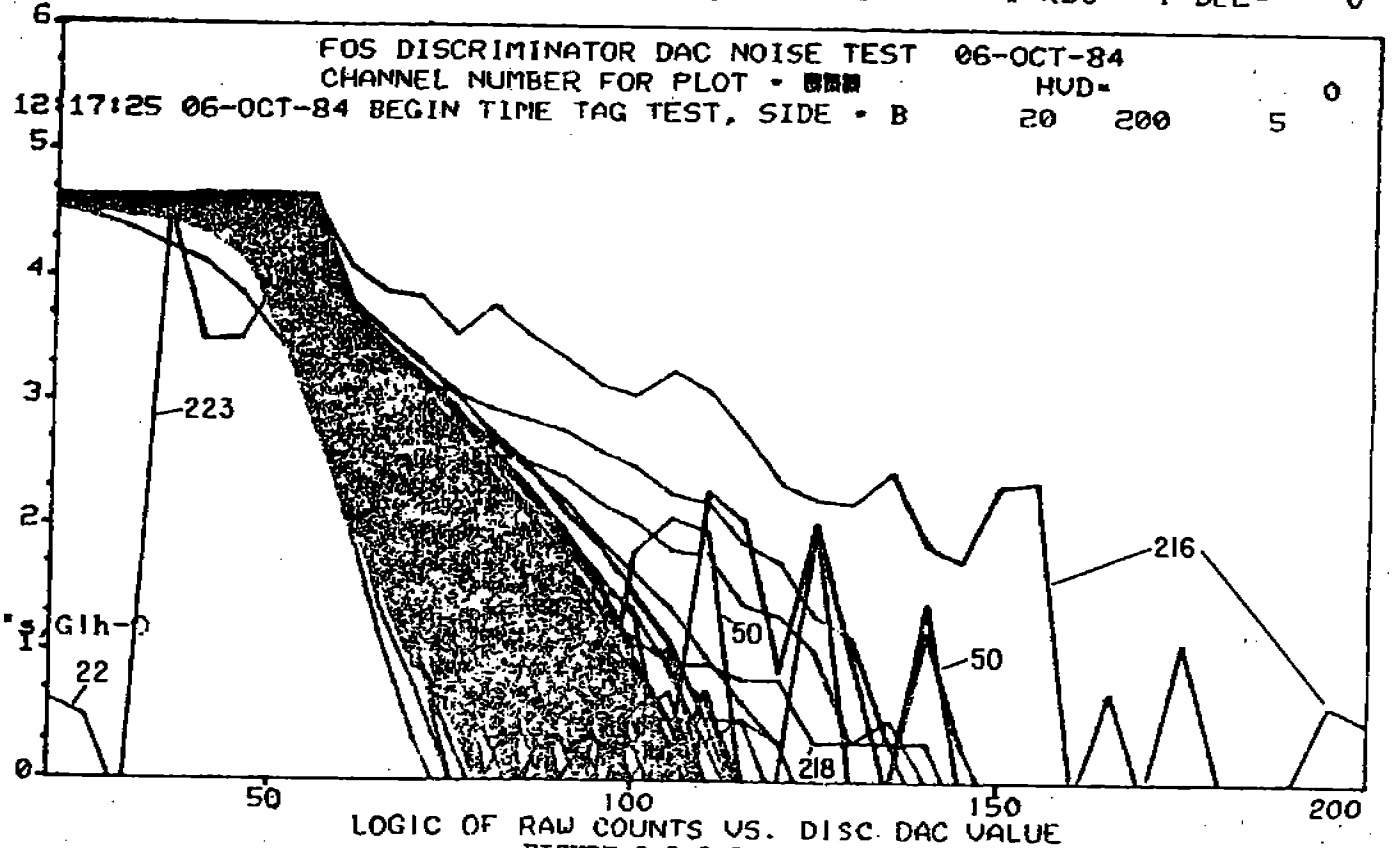

LOGIC OF RAW COUNTS VS. DISC DAC VALUE
FIGURE 3.2.2-2

85EB-11-013

of a set bit in the software. The deperm procedure is basically a 100-step spiral from the maximum x and y deflection step to the center of the format. In this way, the residual external magnetic fields are removed and an acquisition always begins at the same physical position in the image format.

3.3.1.3 Hysteresis Avoidance Calibration - To test the hysteresis avoidance techniques, the following stepping pattern is implemented:

1. +2000 DAC value (+128 diodes) in the x-direction, then deperm procedure back to origin.
2. +2000 DAC value in the x-direction, then back to origin.
3. -2000 DAC value (-128 diodes) in the x-direction, then deperm procedure back to origin.
4. -2000 DAC value in the x-direction, then back to origin.

Figures 3.3.1-1 and 3.3.1-2 are overlays of the positions of the origin for the four separate measurements for each detector as indicated by a chromium line of the internal calibration lamp with the H40 grating.

The shift of approximately 1/2 diode (or 25 microns) right and left of the deperm center is a measure of the maximum hysteresis effect; thus, when the center is established at turn on by the deperm procedure, the hysteresis shift for a deflection is only ~0.8% of the deflection. This is quite acceptable for the standard stepping pattern.

3.3.2 Noise Burst Rejection

X-DEFLECTION_HYSTERESIS_TEST_SIDE=A

```
 DAT 05-OCT-84 HTM 08:11:22 MIF= 49 MAF=      0 BSV=2975 BSI= 324 PSS=  11
EHT=H003XX SDT=H003XX SDF=1  PWD=OK HWC=PFU2 PFS=AMB     TMP=RM   SID=A
CMT  X-DEFLECTION_HYSTERESIS_TEST_SIDE=A          OPR E. W. STREIN
SNC=  165 WPL=  516 LPF=    9 PLZ=CW01 ENT=  2 FGU=H40 APR= C2 TAX=    0
HOV=    0 LOV= 6251 HVD=18359 ARQ= 128 FOC=180 SAF=  0 INM=  0 TAY=    0
XDC=   36 X-P= 1536 X-B=    0 X-9=   8 REF= 71 SLI=  1 MUL=  5 TMX=65535
YDC= 3149 Y-P= 2048 Y-B= -947 Y-9=   1 Y-R= 64 CH1=  0 #CH=512 DE1=    0
LIV=  100 DED=   20 NLM=65535 ACM=   8 INT=  1 PTN=  1 RDO=  1 DE2=    0
  RAW CNTS,YMIN=0.000,YMAX= 30000.0,INTSIZ=1000.0
  DMIN=260,DMAX=377,DAVG=317,ERRONT=  0,ENAB=504,RAMMAP=0,1,2,3,4,5,6,7
```

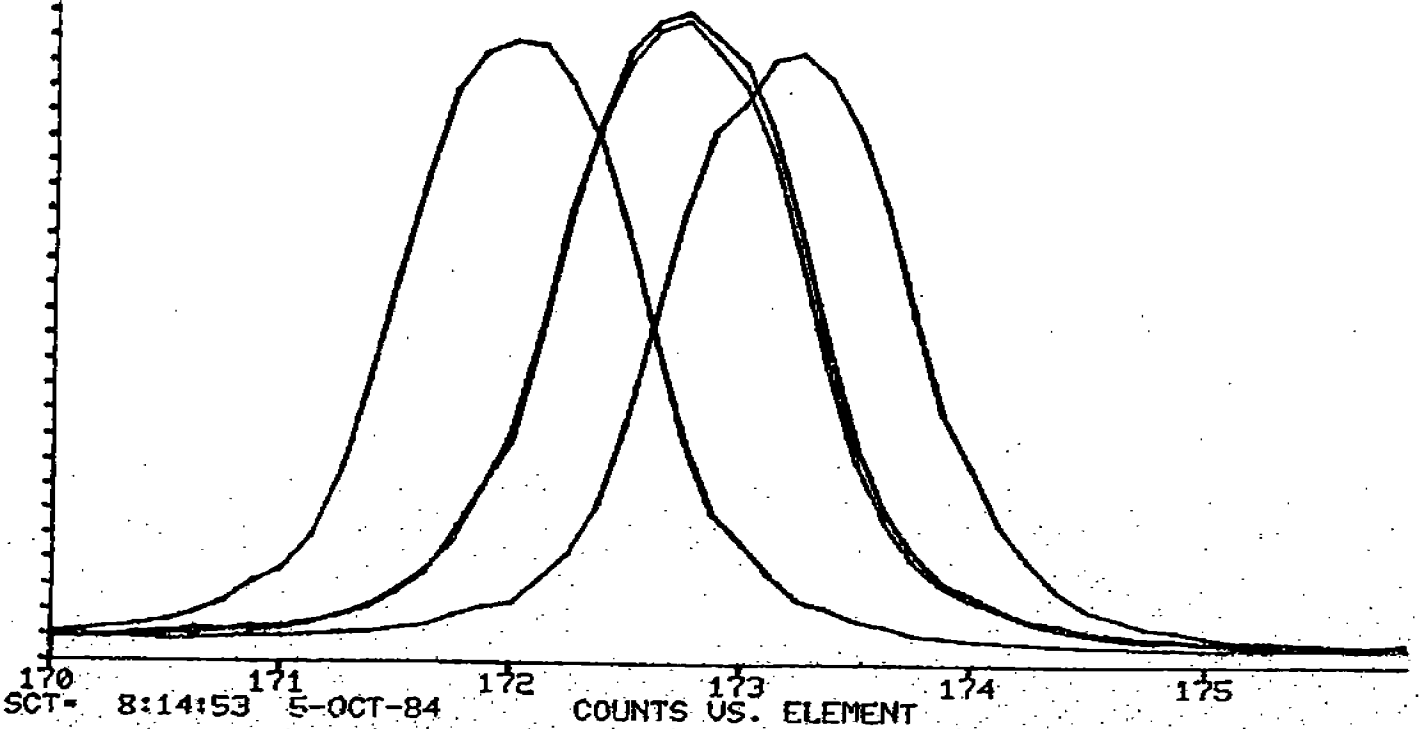

SCT= 8:14:53 5-OCT-84 COUNTS VS. ELEMENT

FIGURE 3.3.1-1

B5EB-II-010

X-DEFLECTION_HYSTERESIS_TEST_SIDE=B

```
 DAT 06-OCT-84 HTM 10:55:14 MIF= 20 MAF=      0 BSU-2974 BSI= 318 PSS=  14
EHT=H003XX SDT=H003XX SDF=1  PWD=OK HWC=PFU2 PRS=AMB    TMP=RM   SID=B
CMT  X-DEFLECTION_HYSTERESIS_TEST_SIDE=B          OPR E. W. STREIN
SNC=  165 WPL=  516 LPF=    9 PLZ=CW01 ENT=  2 FGW=H40 APR= C2 TAX=    0
HOV=    0 LOV=  482 HVD=18353 ARQ= 128 FOO=208 SAF=  0 INM=  0 TAY=    0
XDC=   24 X-P= 1536 X-B=    0 X-S=   8 REF= 71 SLI=  1 MUL=  5 TMX=65535
YDC=  774 Y-P= 2043 Y-B=  774 Y-S=   1 Y-R= 64 CHI=  0 #CH=512 DE1=    0
LIV=  100 DED=   20 NLM=65535 ACM=   8 INT=  1 PTN=  1 RDO=  1 DE2=    0
  RAW CNTS,YMIN=0.000,YMAM= 30000.0,INTSIZ=1000.0
  DMIN=270,DMAX=351,DAVG=316,ERRONT=  1,ENAB=503,RAMMAP=0,1,2,3,4,5,6,7
```

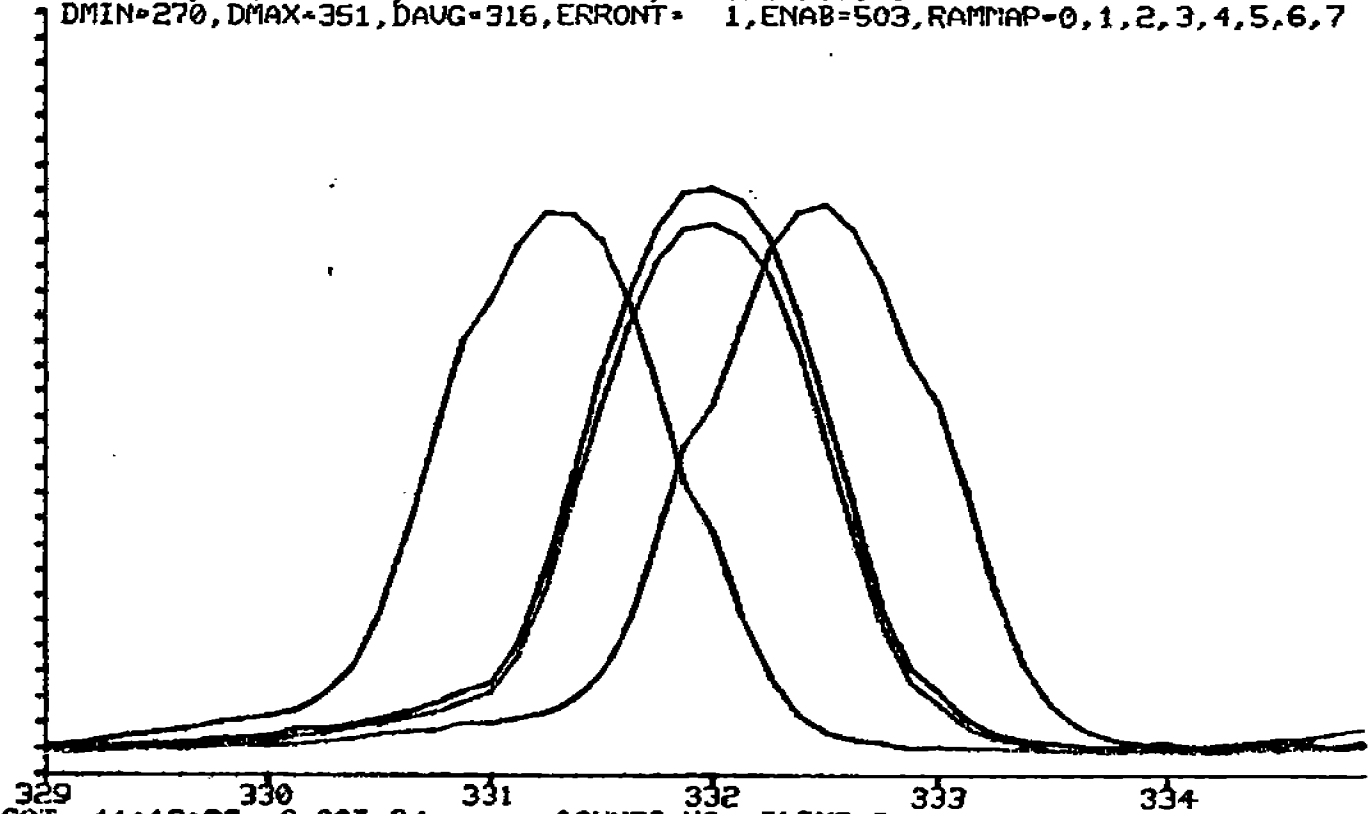

SCT= 11:12:32 6-OCT-84 COUNTS VS. ELEMENT

FIGURE 3.3.1-2

85EB-11-011

Although this feature is used routinely in most FOS data acquisitions, including those forming the database for the calibrations discussed in this report, it was independently tested using an external pulsed lamp. Proper operation was observed in all the reset/retry modes of operation at several thresholds. Essentially, this is not so much a calibration as merely a pass/fail test of the FOS firmware. The unsurprising result was that the firmware operated properly during this test just as it had for the preceding several years.

3.3.3 Time Resolved Modes

The pulsed external lamp was also used to verify the capability of the FOS to add time-phased periodic signals in its internal memory, and to find the maximum rate for which such internal additions can be performed. The frequency of lamp pulses was varied, and data taken for many cycles to determine phase-binning performance. Because the lamp timing was external to the FOS, no absolute phase verification tests could be performed, but several periodicities were tested for operations with noise burst rejection enabled and disabled, with and without the RETRY option, and with both single-precision and double-precision addition. The results agreed with what was expected based on firmware execution timing measurements. In general, exposure rates faster than about 30 per second (accumulation plus readout times exceeding about 30 milliseconds) require caution, and even for single-precision add and RETRY disabled exposure rates cannot exceed about 60 per second (exposure plus readout times around 15 milliseconds) when all 512 diodes are used. We

did not test use of fewer than 512 diodes, although shorter exposure intervals at higher accumulation rates can be obtained with fewer channels. Perhaps more importantly, we could not verify the absolute phasing capability, since we lacked any way to phase lock the external lamp to the FOS firmware. Verification of absolute phase-binning must await on-orbit of pulsars whose absolute phases at the time of the observation are well measured, presumably a calibration that will be undertaken in conjunction with the need to use this rather exotic FOS observing mode.

4.0 TARGET ACQUISITION

Acquiring an extremely faint object with a one-dimensional detector in a viewing field of maximum size 4.3″ square and then centering the object in an aperture as small as 0.1″ is a non-trivial task. To quantify the difficulty, if we require a 95% probability (±2σ) for placing a star in an aperture with a diameter d″, the sum of the pointing errors and relative positional errors must be less than d″/4. Because FOS observations will typically be made with a 0.5″ aperture, and occasionally with 0.25″ and 0.1″ apertures, the positional tolerances are quite stringent. With the additional criterion that the star must be centered well enough to avoid vignetting, the positional tolerance becomes even tighter.

The generic ways to do FOS target acquisition are described in Section 4.1.

4.1 Description of Modes

Acquisition using FOS-provided firmware and software are described in Sections 4.1.1 through 4.1.4. Blind acquisition is discussed in Section 4.1.5 and WF/PC-assisted acquisition in Section 4.1.6.

4.1.1 FOS Imaging

When using the FOS to make a target acquisition image, the 4.3″ x 4.3″ aperture and the camera mirror are selected for the appropriate detector (red or blue). The FOS is then commanded to "map" the aperture by taking a sequence of x-stepped integrations

(nominal x-steps = 4) at different y-deflections. Normally, the 614μ square image of the aperture will be mapped with 12.5μ steps in the y-direction. The sequential target acquisition integrations will be down linked through a TDRSS satellite and sent to the Observer Support System at the STScI. There, the integrations are "stacked" and displayed as a "picture." Because the diodes in the Digicon detectors are 200μ high (1.4″), all stellar images will be 1.4″ long in the y-direction. There exists the option of sharpening the resolution in the x-direction by multiplying the picture by a psuedo-inverse x-restoration matrix (nominally 48 x 51). The y-elongation can be removed by multiplying the picture by a pseudo-inverse y-restoration matrix (nominally 48 x 63). The observer then marks the desired object with a cursor and its measured centroid is used to generate the offset commands which should center the target in a preselected FOS aperture. These commands are uplinked to the HST which then repoints. After (or during) the move, the FOS is reconfigured to the desired setup and the observation begins after the SSM computer sends the appropriate flag to the NSSC-1 computer.

Note that to use the imaging mode for target acquisition, the observer must be at the STScI, and it must be possible to schedule the TDRSS contact in order to get the data down and the offset commands back to the HST. This is also the least efficient target acquisition mode, because the entire aperture must be mapped.

4.1.2 NSSC-1 Binary Search

In principle, the binary search should give the fastest

target acquisition. The binary search program begins by mapping the 4.3" x 4.3" aperture with three y-scans. The mean sky level is calculated at each y-step, and all peaks more than $n\sigma_{sky}$ (nominally n = 3) above the mean sky level and within the count window are noted. The program next uses a binary search pattern to deflect the image of the designated nth brightest peak onto the edge of the diode array. The derived Digicon x and y image coordinates are then converted to scaled microns and transformed into the $\Delta V_2, \Delta V_3$ offset which will center the object in the 4.3" x 4.3" aperture.

The processor includes an extraction of a $\Delta V_2, \Delta V_3$ from the command sequence. This $\Delta V_2, \Delta V_3$ will be the sum of the offset required to select a particular science aperture, and the offset required to move to a faint target if the peak-up was on a bright reference star. This $\Delta V_2, \Delta V_3$ will be added to the $\Delta V_2, \Delta V_3$ derived from the binary search.

If the program fails to find a target, one of three events will occur:

1. If there is no scheduled OSS contact and no preplanned branch, the program will either stop the FOS data acquisition until the allocated time expires, or command a 4.3" move and try again.
2. If there is a scheduled OSS contact, the program will inform OSS that target acquisition failed and wait for the observer to make a decision.
3. If there is a preplanned branch, it will be executed.

4.1.3 Firmware Target Acquisition

The firmware target acquisition will work best for isolated objects. It will measure very accurate positions, and probably will take longer than the more flexible NSSC-1 binary search. The firmware looks for an object within a specified count window. If the firmware finds more than one object within the window, it gives up in confusion; this is after all, a firmware program, and is not meant to do pattern recognition. If the firmware does not find any objects in the window, an FOS processor in the NSSC-1 will respectively raise and lower the upper and lower windows, and command a retry.

The firmware maps the FOS $4.3^{\prime\prime}$ x $4.3^{\prime\prime}$ target acquisition aperture with m y-steps, using x-stepping and overscan at each y-step. The nominal values for x-steps and overscan will be respectively 4 and 8. Although the target acquisition aperture images onto 12 diodes (the scale is 140 microns-arcsec^{-1} and each diode is 50μ x 200μ), the firmware will process the data from 20 diodes. Consequently, the nominal dimensions of the target acquisition data array will be m x (24 x 4) = m x 96. There are 12K words of FOS microprocessor RAM which can be used for target acquisition, which allows commanding up to 120 y-steps, where each step of the 200μ-tall diodes is 5μ ($0.036^{\prime\prime}$). The firmware can be commanded to take any combination of y-steps, x-steps (e.g., 1/8 steps), and overscan as long as the data will fit into the 12K bytes of memory.

The firmware processor includes an option to filter the data array before looking for peaks (stars) in the "picture." The

default x-filtering filters the data array row-by-row with a 5 point isosceles triangle. The default y-filtering filters the data column-by-column with a 7 point piece-wise parabolic smoothing function. Graphically, the function looks like a saw tooth composed of an upright and an inverted isosceles triangle. The x-filter width should be odd with 2n - 1 points, and the y-filter width should be odd with 4n - 1 points. Zero values at the end points are not counted. The filter widths are specified by two serial magnitude commands YXFILWID and YYFILWID.

The objective of the y-filtering is to mark the edge of the diode with a feature which can be accurately centered. If the diodes have a sharp response function at the y-edges, the response to stepping the y-edge across a star will be a step function in the data. The convolution of the filter with a step function gives a piece-wise parabola. Consequently, the two edges of a diode will be marked with parabolas, positive at one end and negative at the other end.

The low pass filtering in x and y will reduce the amplitude of the peaks. The firmware processor has been written such that the data is renormalized after filtering in order to preserve intensity. Because of this care must be used when specifying the data window in which the peak (star) is to be found.

When the "fix bit" is set, the firmware corrects for dead diodes and frames which were rejected because a burst-noise-rejection preset count was exceeded. Fixing the data significantly increases the processing time.

If it is wanted to uplink filter functions which are different than those already described, YFILL and XFILL are set in order to suppress automatic filling of the filter function tables. If the double buffer bit is set, the 12K of memory will be partitioned and the filtered data will be written into the second half of the memory. If the double buffer bit is not set, the filtered data will be written over the unfiltered data. Either filtered or unfiltered data can be read to the NSSC-1.

Note that the y-position is that of the upper edge, center, or lower edge, according to how the target acquisition is specified. If using an edge, the Y-BASE value returned to the NSSC-1 is in "Base units," and is the value which would drive the image to the upper edge of the diode (or center, or lower edge, as the case may be). Appropriate offsets must be applied to the y-position in the NSSC-1.

The processor looks line by line for peaks in the data array which fall within a commandable window. When a peak is found within the window, two parameters, XSKIRT and YSKIRT, are used to see if the peak is a relative maximum. This is accomplished by looking at neighboring peaks out to the distance specified by XSKIRT and YSKIRT. If these parameters have their default values of 1, the 8 nearest points are examined. If a peak is in the window and is a relative maximum, the processor computes its x and y centroid by fitting an isosceles triangle to the peak's x-position and two nearest x-neighbors, and another triangle to the y-position and two nearest y-neighbors.

At the first occurrence of a peak in the window, the processor increments the diagnostic "COUNT" to one. If a second peak is found, the processor uses two parameters to decide if the new peak is part of the same stellar image or a new star. For unfiltered data, the parameters are XPCLOSE and YPCLOSE, with respective default values of 32 (one diode width) and 256 (one diode height).

If the new peak is within XPCLOSE and YPCLOSE of the last peak, count is incremented and the new x and y centroids are averaged with the previous values. If the data has been filtered, the parameters are XPCLOSE and YPCLOSE, with respective default values of 32 and 64. If the new peak is not part of the previous image, the processor sets the "crowded field" bit and quits. In this case, the x and y positions of the new peak are not averaged into the previous x and y positions.

4.1.4 FOS Peak-Up/Peak-Down

When executing a Peak-up/Peak-down target acquisition, the NSSC-1 computer sets parameters or flags which cause the SSM computer to command the HST to step through a preloaded spatial pattern of dwell scans. After the SSM has commanded a small move and the HST has settled, the SSM sets global event flag #2. The NSSC-1 processor picks up this flag and initiates an FOS integration. The completed scan is summed over a specified number of diodes and the sum is saved. The processor records and updates the starting time of the integration which gives either the maximum number of counts (star centered in aperture) or the minimum number of counts (star centered on occulting bar). After the HST

has stepped through the scan pattern, the NSSC-1 computer returns the time of the maximum or minimum sum to the SMM engineering computer. The SSM then repoints the HST to the position which gave the maximum or minimum sum.

4.1.5 FOS Blind Acquisition

Blind acquisition is a blind pointing based on the assumption that the position of the object is accurately known relative to the guide stars used by HST during the observation. Because of the previously stated stringent accuracy requirements, we expect blind acquisition to be used only for revisits to targets whose centered positions are already accurately known relative to the guide stars. A related use of this mode, blind offset pointing, will be often used for acquiring a faint target near a bright star when their separation has been accurately measured.

4.1.6 WF/PC-Assisted FOS Target Acquisition

Some fields such as the centers of globular clusters or active galaxies may be too complex for an FOS target acquisition. In such cases, there are at least two ways to use WF/PC pictures for FOS target acquisition. The first way is to take a WFC or PC picture and then measure the x,y position of the target in the picture relative to an isolated star. The x,y coordinates can then be converted to $\Delta\alpha$, $\Delta\delta$. Subsequently, an offset to the target can be made after an FOS target acquisition on the bright star.

When the HST repoints from the offset star to the target, the FGSs must also move within the FGS fields of view. If one of the guide stars happens to be too close to the edge of the FGS

FOV, the offset might move the star outside the FGS FOV, in which case the offset could not be made. As a rule of thumb, the smaller the distance between the offset star and the target, the more likely it is that two suitable guide stars can be found.

Because the accuracy of the derived relative positions, $\Delta\alpha$, $\Delta\delta$, is not strongly dependent on the accuracy of the HST guide star positions, the first procedure does not require that the FOS observations be made with the same guide stars. Consequently, there are fewer restrictions on when the observations must be made (in order to find suitable guide stars) and the time interval between the WF/PC observations and the FOS observation than if the second method is chosen.

4.2 Current Status

Testing of the FOS target acquisition modes has been an arduous task due to several factors: target acquisition to the accuracy required is inherently difficult; the filter-grating wheel non-repeatability forced us to modify the original procedures by adding internal target acquisition LEDs and suitably updated software in the NSSC-1; and certain target acquisition tests could not be done due to the unavailability of the needed hardware external to the FOS. It was impossible to generate realistic star field simulations of the subarcsecond quality which will be provided by the HST, so the tests used external lamps projected through the FOS entrance apertures to simulate stars; more complex images which simulated multiple stellar

images were generated by dispersing line sources onto the detectors.

The capability of the FOS to image regions of the photocathode (the target acquisition mode described in Section 4.1.1) has been amply verified in numerous y-maps. The software to display the data, generate offsets, and uplink slew commands is completely external to the FOS and thus no tests of this mode are discussed in this document. Similarly, the modes described in Section 4.1.5 (blind acquisition) and Section 4.1.6 (WF/PC-assisted acquisition) are not amenable to FOS instrument-level tests. Crude tests and computer simulations of the peak-up/peak-down acquisition mode (Section 4.1.4) have been made; however, in this mode, the "intelligence" of the acquisition lies in the HST computers, since the FOS simply provides the data which the SSM uses to correlate with the desired spatial position from its slew pattern.

Section 4.2.1 discusses the test results of the internal FOS firmware, which performs the target acquisition described in Section 4.1.3. The tests of the recently changed binary search target acquisition, described in Section 4.1.2, are discussed in some detail in Section 4.2.2. Finally, Section 4.2.3 describes the use of onboard LEDs for target acquisition and plans for tests within the next few months on the recently installed LEDs which will be used to support target acquisition for the binary search and firmware modes.

4.2.1 Firmware Acquisition Tests

4.2.1.1 Test Description

The FOS firmware target acquisition was tested June 24, 1984 at Martin Marietta during the ambient calibration. The tests were made with the UV STOS and Argon lamp on the blue side using aperture B2(0.3" circular). We ran four manual Y-maps with 1/4 X-step, varying Y-base, Y-range, and the Y-step size from one map to the next. The first Y-map was used to locate the X and Y positions of the aperture B2. The data from the next three aperture maps were used by the firmware to locate the aperture.

4.2.1.2 Test Results

1. Position of the aperture B2, based on hand reductions during the test.

   Y-Base = -532
   Y-Range = 30
   Y-Step = 68 (16μ/step)
   X Center = 236.95 = -610 DACs relative to the center diode #256.
   Y Center = Step #18.4 = -272 DACs below center.

2. Firmware Positions of B2.

Test No.	Y-B	Y-R	Y-S	Y-Step Size	Upper Edge X cent.	Upper Edge Y cent.	Lower Edge X cent.	Lower Edge Y cent.
2	-532	10	68	8	-610	-374	-611	-167
3	-448	8	16	16	-609	-373		
4	-500	16	16	32	-609	-372	-610	-166

The scale conversion between DAC units and microns on the photocathode is not known to better than one or two percent. If we assume 1 DAC unit = 1μ, the upper edge gives a maximum error of 2μ relative to the center of the 200μ tall diodes, for step sizes as large as 32μ. The lower edge gives errors of 3μ and 5μ. If we use a sequence of tests such as this to define the DAC to

microns conversion, the Y-centering may be even more accurate than 2 or 3 microns.

The microprocessor processing time for 16 lines of data and filtering is about 48 seconds.

4.2.1.3 Test Summary

FOS firmware target acquisition can find the X position of a "star" to ~ 1 micron and the Y-position to an accuracy of at least 3 microns.

4.2.2 Binary-Search Tests

4.2.2.1 February 1986 Test

For the NSSC-1 binary search target acquisition tests of February 1986, a star field was simulated by using a platinum lamp, the double 0.1″ aperture, and the G190H grating. By processing diodes 270 through 286, this configuration resulted in a pseudo-star field containing six point sources. These sources are made up of the lines at 1907.493, 1911.702, and 1916.083 Å which are imaged once in each aperture. Using the NSSC-1, the test then attempted to find one of these sources and put it on the edge of the diode array.

For the binary search test, three of the parameters varied, YNBRT, NMAX, and NMIN. Each setting of parameters was tested with three different starting values of YBASE. Of the 16 cases run, five failed due to incorrect YBASES and an additional four failed because there were not enough y steps to put the target on the edge. These problems have been corrected; YBASE apparently needed a longer wait time when initially set in a binary search sequence, and the maximum number of y steps has been increased

from five to eight. One additional case was run with NMAX and NMIN set to exclude all sources in the field. This case failed in the correct way, that is, the correct value of YGIVUP = 10 was returned.

The binary search centering accuracy in the y direction is a function of the maximum count rate and the response of the diode edge to a point source. We do a linear fit to the data to show that the slope at half of the peak signal is 3% of the response. Using this value, achieving y centering to 1 micron accuracy with $\pm$ 3σ certainty requires that the sum of the counts per y step exceed 5000.

The target acquisition test showed that in general the software logic was correct and working. To rectify the problem with YBASEs, changes have been made in the target acquisition procedure (proc) and to rectify the problem with y steps, changes have been made in the flight software. The proposed target acquisition test of August 1985 will check that these changes have been correctly implemented.

Table 4.2.2.1-1 summarizes the target acquisition test.

4.2.2.2 <u>August 1985 Tests</u>

The binary search target acquisition tests at Lockheed Missiles and Space Company were run under the new flight software, version 3.6. Several important changes had been made in the 3.6 software, as well as a number of smaller, more technical changes: (1) the maximum number of binary search steps is now eight rather than five; (2) finding more than four sources in one Y strip in the new version causes an exit and an error message to

TABLE 4.2.2.1-1

Target Acquisition Test: February, 1985

Case	YNBRT	NMAX	NMIN	YBASE	Result
1	1	2000	200	36	successful
2	1	2000	200	?	wrong YBASE
3	1	2000	200	10	needed more y steps
4	2	2000	200	36	needed more y steps
5	2	2000	200	62	successful
6	2	2000	200	?	wrong YBASE
7	3	2000	45	36	needed more y steps
8	3	2000	45	62	successful
9	3	2000	45	62	successful
10	4	2000	45	?	wrong YBASE
11	4	2000	45	62	successful
12	4	2000	45	10	successful
13	3	50	10	?	wrong YBASE
14	3	50	10	?	wrong YBASE
15	3	50	10	10	successful
16	1	40,000	30,000	44	successful

be written rather than causing an abort; and (3) an integer overflow (counts in excess of $2^{16} - 1$) is flagged by setting the counters to the maximum value rather than simply letting the counters reset to zero.

As with the target acquisition tests of February 1985, a star field was simulated by using a platinum lamp in the 0.3" aperture with the G190H grating. This was done on the blue side because the red tube had been removed for replacement. By processing diodes 214 through 238, this configuration resulted in a pseudo-star field with three stars which are made up of the lines at 1907.493, 1911.702, and 1916.083 Å. The NSSC-1 FOS Binary Search Flight Software test searched for a specified source and measured its Y position by deflecting it on the Y edge of the diode array. A fine map in both X and Y was done before and after the test in order to have an independent measure of the correct position. These maps are shown in Figures 4.2.2.2-1 through 4.2.2.2-3. Twenty-one test cases were run using various settings of the binary search parameters and testing various alternative branches.

The test cases were run three times, with a high fail rate the first two times due to a timing problem with the turn on of the calibration lamp. The final run of the twenty-one test cases was done with the lamp left on through each test case, and this run was completely successful. The results of the final run of August 20, 1985 are summarized in Tables 4.2.2.2-1 and 4.2.2.2-2 and discussed in more detail below. The first fourteen cases are completely described in Table 4.2.2.2-3, with the Y-BASE

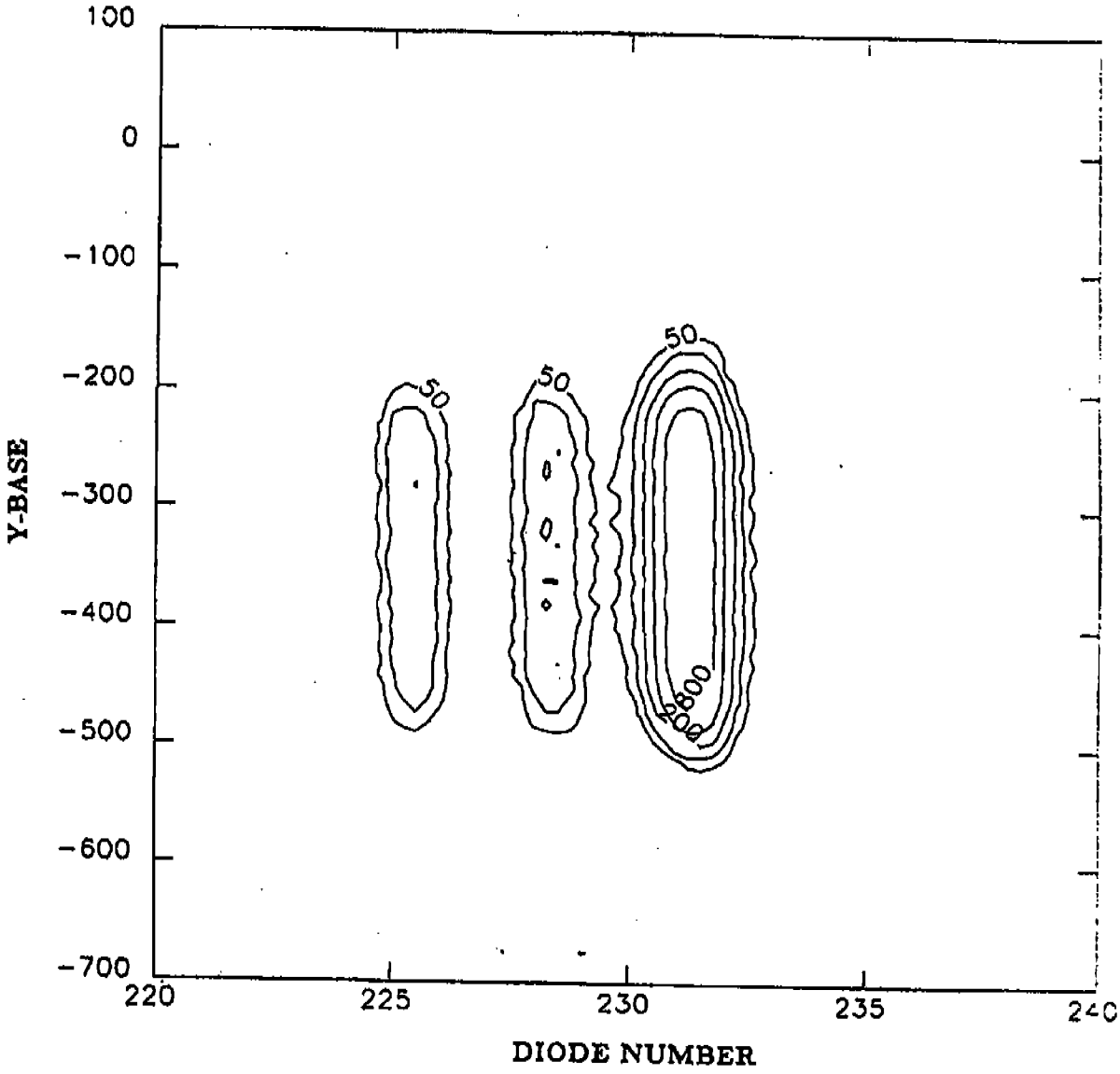

Figure 4.2.2.2-1. Simulated 4".3 star field using platinum lamp through 0".3 aperture

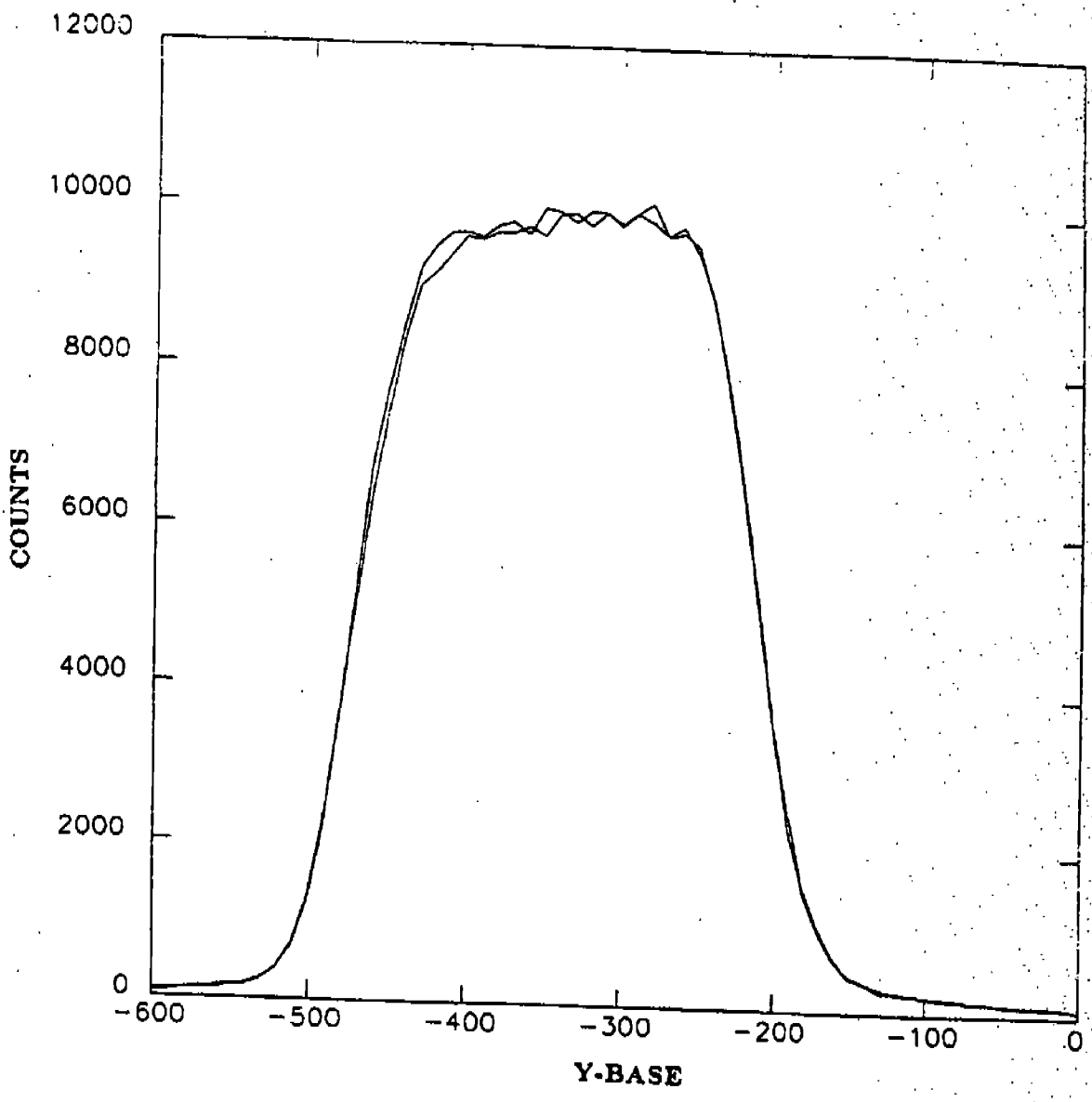

Figure 4.2.2.1-2. Profile of Y scan before and after target acquisition

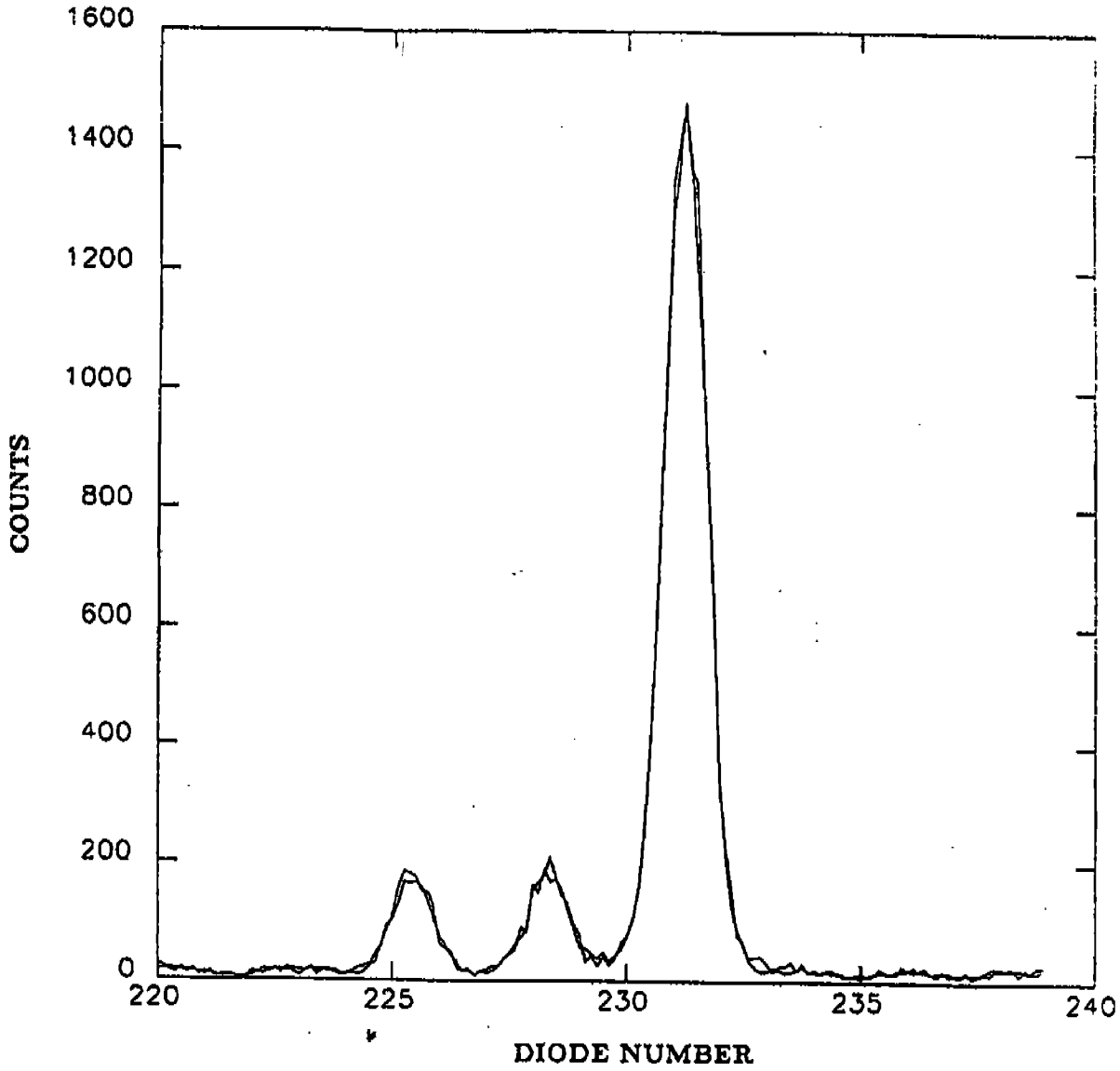

Figure 4.2.2.1-3. Profile of Y scan before and after target acquisition

TABLE 4.2.2.2-1

Parameters for Binary Search TA Tests: LMSC, August, 1985

Case	YBASE	YTOLER	YSTAT	YNMAX	YNMIN	YNBRT	YPPB
1	-1121	3	200	2000	64	1	2
2	-993	3	200	2000	64	1	2
3	-1200	3	200	2000	64	1	2
4	-1100	3	0	2000	64	1	2
5	-1050	3	0	2000	64	1	2
6	-1249	3	0	2000	64	1	2
7	-1140	6	0	2000	64	1	2
8	-1020	6	0	2000	64	1	2
9	-1170	6	0	2000	64	1	2
10	-1080	3	200	2000	64	2	2
11	-1070	3	200	2000	64	2	2
12	-1235	3	200	2000	64	2	2
13	-1110	3	200	2000	64	3	2
14	-1040	3	200	2000	64	3	2
15	-1180	3	200	2000	64	3	2
16	-1102	3	200	60000	50000	1	2
17	-910	3	200	2000	100	1	2
18	-1358	3	200	2000	3	1	2
19	-1102	3	200	2000	1997	1	1
20	-910	3	200	2000	1997	1	1
21	-1102	-	-	-	-	-	-

Notes: The numbers are quoted in decimal but inserted in procs in octal.

TABLE 4.2.2.2-2

Results of Binary Search TA Tests: LMSC, August, 1985

Case	YGIVUP	BS Steps	YFXCTR	YFYCTR	Result
1	0	5	113.313	-185.625	Succeeded
2	0	5	114.094	-185.625	Succeeded
3	0	5	113.719	-185.844	Succeeded
4	0	7	113.313	-183.281	Succeeded
5	0	8	112.531	-185.625	Succeeded
6	0	7	113.313	-184.063	Succeeded
7	0	6	112.938	-184.844	Succeeded
8	0	6	114.094	-184.844	Succeeded
9	0	6	113.313	-183.281	Succeeded
10	0	4	-32.375	-184.844	Succeeded
11	0	4	-30.031	-177.031	Succeeded
12	0	4	-20.281	-180.938	Succeeded
13	0	4	-177.281	-183.281	Succeeded
14	0	5	-175.719	-184.844	Succeeded
15	0	4	-176.906	-187.969	Succeeded
16	10	-	-	-	Failed correctly
17	0	5	NA	-183.281	Succeeded
18	5	-	-	-	Failed correctly
19	9	-	-	-	Raster scan enabled
20	-	-	-	-	Pre-planned branch
21	-	-	-	-	Peak-up

Notes: YGIVUP is set upon completion of BS TA. 0 means the source was successfully placed on the edge of the aperture. 5 means that more than 4 stars were found in a Y strip. 9 means that AP 32 ran out of moves for a raster scan without finding the target and 10 means that nothing was found.

TABLE 4.2.2.2-3

Summary of Test Cases

Case 1	Y-BASE	YNTARG	ON ARRAY	YNMAX
Ap Map	-300			6670
	-556			
	-44			
BS	-172	515	NO	
	-236	5707	YES	
	-204	2711	NO	
	-220	4084	YES	
	-212	3347	ON EDGE	
Results:	YFXCTR=113.313	ΔX=1.06	YFYCTR=-185.625	ΔY=1.80

Case 2	Y-BASE	YNTARG	ON ARRAY	YNMAX
Ap Map	-172			6626
	-428			
	-84			
BS	-300	6791	YES	
	-236	5912	YES	
	-204	3626	NO	
	-220	4341	YES	
	-212	3449	ON EDGE	
Results:	YFXCTR=114.094	ΔX=0.26	YFYCTR=-185.625	ΔY=1.80

Note: X and Y postions are given in units of microns at the photocathode.

TABLE 4.2.2.2-3 CONT'D

Case 3	Y-BASE	YNTARG	ON ARRAY	YNMAX
Ap Map	-379			6726
	-635			
	-123			
BS	-251	6434	YES	
	-187	1266	NO	
	-219	4250	YES	
	-203	2596	NO	
	-211	3330	ON EDGE	
Results:	YFXCTR=113.719	ΔX=0.66	YFYCTR=-185.844	ΔY=2.01

Case 4	Y-BASE	YNTARG	ON ARRAY	YNMAX
Ap Map	-279			
	-535			6599
	-23			
BS	-151	183	NO	
	-215	3820	YES	
	-183	1055	NO	
	-199	2292	NO	
	-207	2851	NO	
	-211	3403	YES	
	-209	3237	ON EDGE	
Results:	YFXCTR=113.313	ΔX=1.06	YFYCTR=-183.281	ΔY=-0.55

TABLE 4.2.2.2-3 CONT'D

Case 5	Y-BASE	YNTARG	ON ARRAY	YNMAX
Ap Map	-299			7038
	-485			
	27			
BS	-101	57	NO	
	-165	378	NO	
	-197	1952	NO	
	-213	3627	YES	
	-205	2803	NO	
	-209	3182	NO	
	-211	3267	NO	
	-212	3575	ON EDGE	
Results:	YFXCTR=112.531	ΔX=1.84	YFYCTR=-185.625	ΔY=1.80

Case 6	Y-BASE	YNTARG	ON ARRAY	YNMAX
Ap Map	-428			6710
	-684			
	-172			
BS	-300	6854	YES	
	-236	5810	YES	
	-204	2676	NO	
	-220	4274	YES	
	-212	3572	YES	
	-208	3125	NO	
	-210	3340	ON EDGE	
Results:	YFXCTR=113.313	ΔX=1.06	YFYCTR=-184.063	ΔY=0.23

TABLE 4.2.2.2-3 CONT'D

Case 7	Y-BASE	YNTARG	ON ARRAY	YNMAX
Ap Map	-319			6617
	-575			
	-63			
BS	-191	1548	NO	
	-255	6544	YES	
	-223	4674	YES	
	-207	2968	NO	
	-215	3925	YES	
	-211	3410	ON EDGE	
Results:	YFXCTR=112.938	ΔX=1.44	YFYCTR=-184.844	ΔY=1.01

Case 8	Y-BASE	YNTARG	ON ARRAY	YNMAX
Ap Map	-199			
	-455			6995
	57			
BS	-327	6698	YES	
	-263	6769	YES	
	-231	5376	YES	
	-215	3844	YES	
	-207	3127	NO	
	-211	3373	NO EDGE	
Results:	YFXCTR=114.094	ΔX=0.28	YFYCTR=-184.844	ΔY=1.01

TABLE 4.2.2.2-3 CONT'D

Case 9	Y-BASE	YNTARG	ON ARRAY	YNMAX
Ap Map	-349			6681
	-605			
	-93			
BS	-221	4459	YES	
	-157	233	NO	
	-189	1468	NO	
	-205	2847	NO	
	-213	3675	YES	
	-209	3242	ON EDGE	
Results:	YFXCTR=113.313	ΔX=1.06	YFYCTR=-183.281	ΔY=-0.55

Case 10	Y-BASE	YNTARG	ON ARRAY	YNMAX
Ap Map	-259			722
	-515			
	-3			
BS	-131	50	NO	
	-195	243	NO	
	-227	590	YES	
	-211	408	ON EDGE	
Results:	YFXCTR=-32.375	ΔX=-0.13	YFYCTR=-184.844	ΔY=1.01

TABLE 4.2.2.2-3 CONT'D

Case 11	Y-BASE	YNTARG	ON ARRAY	YNMAX
Ap Map	-249			657
	-505			
	7			
BS	-121	34	NO	
	-185	177	NO	
	-217	416	YES	
	-201	289	ON EDGE	
Results:	YFXCTR=-30.031	ΔX=-2.47	YFYCTR=-177.031	ΔY=-6.80

Case 12	Y-BASE	YNTARG	ON ARRAY	YNMAX
Ap Map	-414			727
	-670			
	-158			
BS	-286	756	YES	
	-222	528	YES	
	-190	216	NO	
	-206	380	ON EDGE	
Results:	YFXCTR=-20.281	ΔX=-12.22	YFYCTR=-180.938	ΔY=-2.59

TABLE 4.2.2.2-3 CONT'D

Case 13	Y-BASE	YNTARG	ON ARRAY	YNMAX
Ap Map	-289			643
	-545			
	-33			
BS	-161	35	NO	
	-225	429	YES	
	-193	161	NO	
	-209	329	ON EDGE	
Results:	YFXCTR=-177.281	ΔX=-0.72	YFYCTR=-183.281	ΔY=-0.55

Case 14	Y-BASE	YNTARG	ON ARRAY	YNMAX
Ap Map	-219			761
	-475			
	37			
BS	-91	24	NO	
	-155	15	NO	
	-187	119	NO	
	-203	251	NO	
	-211	354	ON EDGE	
Results:	YFXCTR=-175.719	ΔX=-2.28	YFYCTR=-184.844	ΔY=1.01

values of each Y strip, the total counts in the source (YNMAX), the total counts in the source at any binary step (YNTARG), the final result in microns at the photocathode (YFXCTR and YFYCTR), and difference between that and the value we calculate by hand from the fine maps in X and Y (ΔX and ΔY).

We tested the binary search algorithms by changing the settings of Y-BASE, the settings of the tolerances for putting an object on the edge of the diode array, and the settings for YNBRT. Binary search succeeded for all values of Y-BASE, including Y-BASE such that the star started on the edge between two Y strips (case 5). Although some of the tolerances for putting the star on the edge were more stringent than others, there was no significant difference in the accuracy achieved. Cases 1 through 3, 4 through 6, and 7 through 9 had different tolerance settings, yet there is little indication that the most stringent setting (cases 4 through 6) resulted in a higher accuracy. However, as soon as a dimmer star is used as the acquisition object, as with YNBRT of 2 or 3 in cases 10 through 15, the accuracy goes down appreciably.

We also tested the option to have a raster scan and a preplanned branch by causing the binary search to fail. Both options worked as expected.

As can be seen in Table 4.2.2.2-2, the changes to flight software have been made correctly. The number of binary search steps exceeds 5 in most cases and in at least one case goes up to the maximum value of 8. Also, case 18 was set with a very broad window for finding peaks, so that too many peaks would be found

in any Y strip. This case resulted in a YGIVUP value of 5, indicating that more than 4 peaks had been found. The more technical changes to the flight software were verified to have been made correctly, with the exception of integer overflow, which still remains to be tested.

In summary, the tests of binary search target acquisition with version 3.6 of the flight software, done at LMSC in August of 1985, were completely successful. They verified not only that the changes to the flight software had been made correctly, but also that target acquisition worked in the way that was originally envisioned and all the options were operating correctly. The bright targets were acquired within $\pm$ 2μ in X and Y. Considering that the dimension of the smallest FOS aperture (0.1) is 14μ in the image plane, this is a very acceptable accuracy.

4.2.3 Use of Onboard LEDs

Because of the non-repeatability of the filter-grating wheel, most target acquisitions will be carried out in a two-step process; first the target will be acquired with whatever software is most appropriate, and then the aperture will be acquired with the same software by turning on the LED, meanwhile leaving the camera mirror in place.

This process will be emulated for TA tests in the following way. A paired aperture will be illuminated by the LED with the camera mirror in place. Target acquisition will be done on the lower of the pair using either binary search or firmware. The result of that acquisition is labeled in the schematic below as SLEW 1. Then a single aperture will be rotated in, and an acqui-

SCHEMATIC - Emulation of Target Acquisition Test

Step 1: The paired aperture is illuminated by the LED, with the camera mirror in place. A target acquisition is performed using the lower square aperture as the target. The result is a slew request to put the target into the supposed center of the large aperture (SLEW 1).

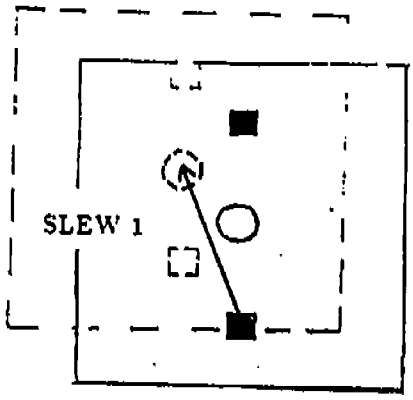

Step 2: The circular aperture is illuminated by the LED with the camera mirror still in place. An aperture acquisition is performed. The result is a slew request to put the supposed center of the large aperture onto the real center of the large aperture (SLEW 2).

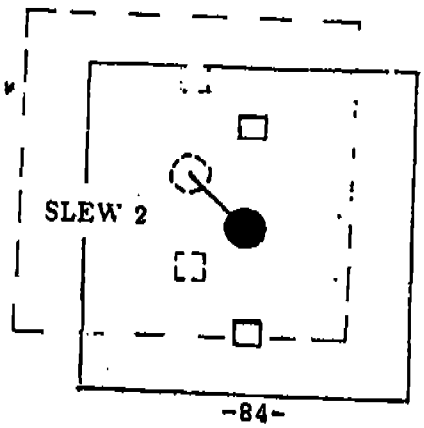

The summation of SLEW 1 and SLEW 2 is D, the distance between the two apertures.

$$SLEW1 + SLEW2 = D$$

This mimics a real target acquisition, where SLEW 1 plus SLEW 2 is the distance from the target to the science aperture.

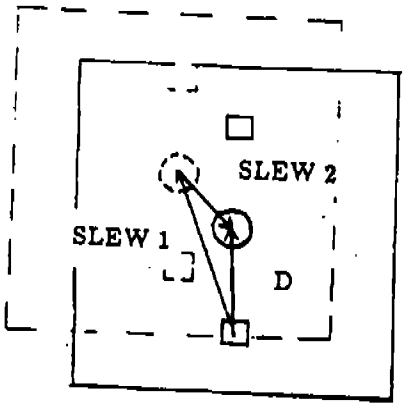

sition of the aperture will be done, again using either binary search or firmware. Since this is an aperture acquisition, the result is a slew from the known position of the aperture to the believed position of the aperture, labeled SLEW 2 in the schematic. This allows a simple check of the two step target acquisition, since SLEW 1 plus SLEW 2 is the distance between the two apertures. This is also illustrated in the schematic.

With the insertion of the LEDs into the FOS, calibration was done to determine the illumination level and uniformity over the 4.3″ square aperture.

The net result is that the large aperture is illuminated in a non-uniform way on both the red and the blue side. It is therefore very important to test the accuracy of the aperture acquisition for all science apertures.

This can be done by performing target acquisition on the lower 0.1″ aperture, followed by aperture acquisitions using the circular 0.3″, 0.5″, and 1.0″ apertures, respectively. Then the target acquisition can be done on the 0.3″ circular aperture, followed by aperture acquisitions in the lower square 0.25″, 0.5″, and 1.0″ apertures, respectively. In order to evaluate the accuracy of our results, aperture maps should be done before the first target acquisition and the first aperture acquisition. The entire sequence is summarized in Table 4.2.3-1.

This sequence (1 aperture map, 1 target acquisition, 1 aperture map, 3 aperture acquisitions, 1 target acquisition, and 3 aperture acquisitions) will be carried out with both the binary

TABLE 4.2.3-1

Target Acquisition Test Sequence

	Function	Aperture	Result
1.	Aperture Map	lower paired 0".1	Map of 0".1
2.	Target Acq	lower paired 0".1	SLEW 1
3.	Aperture Map	circular 0".3	Map of 0".3
4.	Aperture Acq	circular 0".3	SLEW 2
5.	Aperture Acq	circular 0".5	SLEW 2
6.	Aperture Acq	circular 1".0	SLEW 2
7.	Target Acq	circular 0".3	SLEW 1
8.	Aperture Acq	lower paired 0".25	SLEW 2
9.	Aperture Acq	lower paired 0".5	SLEW 2
10.	Aperture Acq	lower paired 1".0	SLEW 2

Note: This sequence must be done with both binary search and firmware. The two methods of acquisition must be tested on both the red and the blue sides. This means performing the above sequence four times.

search algorithm and with the firmware. This must be done for both the red and the blue sides, so that the entire sequence must be done four times.

When the preceding tests are completed, a simple test of the accuracy of binary search TA will also be done. This can be run with the LED illuminating the lower paired 0.1" aperture and using a series of decreasing integration times, so that the total counts in the peak decrease from 3000, to 1500, 750, 325 and 112. This test will give us experience with binary search accuracy that will be invaluable in planning target acquisitions.

These tests were planned for February 1986 at LMSC.

5.0 SPECTRAL CALIBRATION

5.1 Scale and Dispersion

Two internal Pt-Cr-Ne vacuum data sets obtained using the A4 (0.1 arcsec) lower aperture were available for wavelength calibrations. Third order polynomials were fit to all gratings except L65 on the blue side and L15 on the red side which had too few unblended reference lines to properly constrain a cubic fit. Figure 5.1-1 is an example of an FOS spectrum used for this analysis. Figure 5.1-2 shows systematic residuals for a linear fit and motivates the use of cubic fits. The coefficients of the polynomial fit for all gratings and the prism are listed in Table 5.1-1 for the blue Digicon and in Table 5.1-2 for the red Digicon. Table 5.1-3 lists the wavelength range and average dispersion for each disperser. The RMS scatter of the residuals for the high dispersion gratings ranges from .023 pixels to .054 pixels on the blue side and from .023 pixels to .041 pixels on the red side (Tables 5.1-1 and 5.1-2; Figure 5.1-3). The RMS scatter for grating L15 is about .067 pixels for both sides and for L65 it is .36 pixels on the blue side (linear fit) and .022 on the red side (cubic fit). The prism was fit by a fourth order expansion in 1/x with a RMS residual of .2 pixels (see Figures 5.1-4 and 5.1-5). For gratings H27 and H40, there is a systematic residual in the fits for the blue detector. Fifth order polynomials only reduced the RMS error from .038 pixel to .031 pixel for H27 and from .047 pixel to .035 pixel for H40. A scatter diagram depicting the residuals from H27 and H40 on the

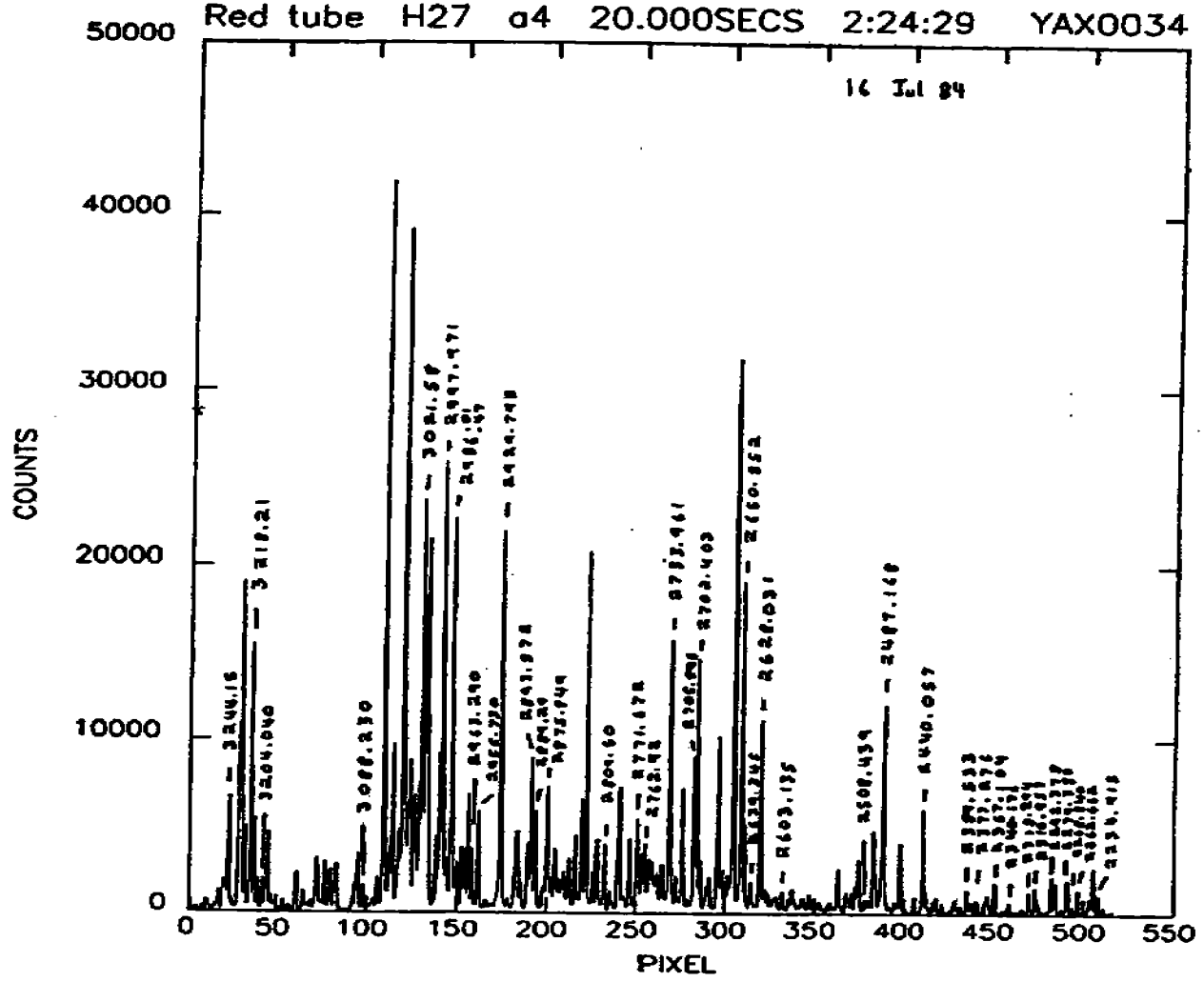

Figure 5.1-1. Typical FOS calibration spectrum. This plot is from the red Digicon; grating H27; aperture a4 (0.1 arcsec). The lines that are labeled with their air wavelengths in Å are used for the dispersion relation calculations after converting to vacuum wavelengths.

TABLE 5.1-1

RED TUBE DISPERSION COEFFICIENTS

16 JULY 84

GRATING	A	B	C	D	SIGMA(px)
H19	2322.513	-1.45718	6.58573E-6	4.43439E-9	.032
H27	3292.711	-2.07717	7.25595E-6	1.07575E-8	.028
H40	4802.383	-3.04342	5.40444E-6	1.91643E-8	.023
H57	6849.174	-4.42790	1.04729E-5	2.16783E-8	.030
H78	9259.337	-5.79737	-2.36782E-5	8.16690E-8	.023
L15	2473.402	-6.95873	0.0	0.0	.067
L65	8904.327	-25.1923	1.05742E-3	-1.52250E-6	.018

17 JULY 84

H19	2322.212	-1.45708	2.20500E-6	1.10397E-8	.041
H27	3292.243	-2.07911	1.05702E-5	7.67617E-9	.029
H40	4802.257	-3.04698	1.51817E-5	8.74792E-9	.022
H57	6848.519	-4.43086	1.67005E-5	1.26003E-8	.032
H78	9261.217	-5.79513	-3.58795E-5	9.19218E-8	.023
L15	2471.840	-6.96511	0.0	0.0	.067
L65	8895.502	-25.1598	8.08459E-4	-1.13636E-6	.022

PRISM 13 JULY 84

X	A0	A1	A2	A3	A4
497.634	1151.56	-1.81268E+5	-2.67773E+6	-3.94582E+7	-2.25992E+8

PRISM 19 JULY 84

497.158	1159.08	-1.29537E+5	-2.60048E+6	-3.70814E+7	-2.05205E+8

$$\lambda_c = A + B(PX) + C(PX)^2 + D(PX)^3$$

$$\lambda_p = A0 + \frac{A1}{(PX-X)} + \frac{A2}{(PX-X)^2} + \frac{A3}{(PX-X)^3} + \frac{A4}{(PX-X)^4}$$

TABLE 5.1-2

BLUE TUBE DISPERSION COEFFICIENTS

13 JULY 84

GRATING	A	B	C	D	SIGMA(px)
H13	1090.385	.99652	4.86964E-5	-7.13150E-8	.023
H19	1575.250	1.47056	3.43885E-5	-7.55204E-8	.038
H27	2226.658	2.10005	3.62150E-5	-9.35269E-8	.038
H40	3244.323	3.07613	5.53993E-5	-1.38085E-7	.047
H57	4583.391	4.47959	5.72694E-5	-1.73970E-7	.048
L15	-838.888	5.32069	3.93095E-3	-3.12077E-6	.069
L65	-4268.643	27.4908	0.0	0.0	.36

19 JULY 84

H13	1090.334	1.00116	3.31290E-5	-5.59020E-8	.026
H19	1575.893	1.47067	3.37199E-5	-7.58713E-8	.032
H27	2227.256	2.10037	3.29076E-5	-8.94733E-8	.042
H40	3248.346	3.07326	6.82611E-5	-1.56275E-7	.054
H57	4588.035	4.47360	1.00810E-4	-2.68694E-7	.045
L15	-954.675	6.15569	2.02297E-3	-1.68022E-6	.061
L65	-4251.534	27.4830	0.0	0.0	.36

PRISM 13 JULY 84

X	AO	A1	A2	A3	A4
-9.49161	967.797	1.93746E+5	-7.33516E+6	3.88529E+8	-6.07318E+9

PRISM 19 JULY 84

-12.3487	971.288	1.92643E+5	-6.86636E+6	3.77518E+8	-5.52079E+9

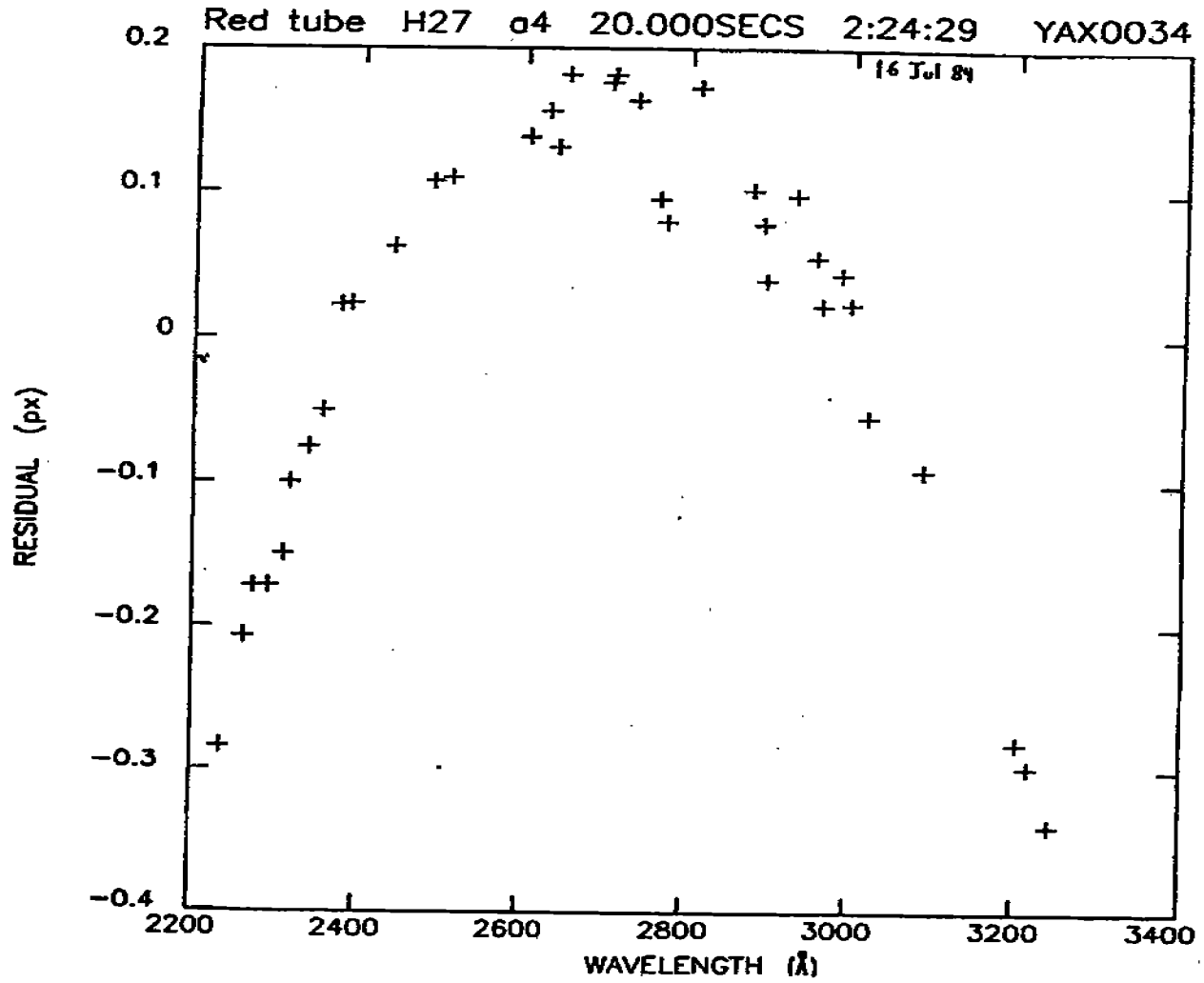

Figure 5.1-2. Plot of residuals to a linear fit (in pixels) vs. wavelength for grating H27, red Digicon. Note the systematic curvature.

TABLE 5.1-3

WAVELENGTH COVERAGE OF FOS DISPERSERS AND AVERAGE DISPERSIONS WITH MAXIMUM DEVIATIONS FROM THE MEAN

RED TUBE

GRATING	LOW(Å)	HIGH(Å)	DISP(Å/px)	MAX DEV(%)
H19	1573[a]	2323	-1.4527	.385
H27	2225	3293	-2.0707	.442
H40	3237	4802	-3.0357	.411
H57	4571	6849	-4.4170	.370
H78	6274	9259	-5.7882	.511
L15	1600[b] (Px 124)	2473[c]	-6.9587	0.0
L65	3850 (Px 202)	8904[d]	-25.0509	.599
PRI	1850[e] (Px 332)	5500 (Px 485)		

BLUE TUBE

H13	1150[a] (Px 60)	1608	1.0027	1.16
H19	1575	2332	1.4880	1.46
H27	2227	3306	2.0942	1.40
H40	3244	4827	3.0685	1.38
H57	4583	6885[f]	4.4636	1.33
L15	1150[a] (Px 318)	2523[c]	6.5023	2.43
L65	3850 (Px 345)	9910[d,f]	27.4908	0.0
PRI	1850[e] (Px 175)	5500 (Px 25)		

All wavelengths are for the extreme pixel values of 0 and 516 except as noted.

[a] MgF_2 cutoff is at 1150Å.

[b] The red tube's quartz window begins to attenuate strongly below 1750Å. See the absolute photometric calibration curves for the amount of attenuation.

[c] Second order overlaps first order longward of 2300Å.

[d] Second order overlaps first order longward of 7900Å.

[e] Sapphire cutoff is 1650Å, but because of the large dispersion of the prism at the shortest wavelengths, the effective cutoff is longward of 1650Å (see the absolute photometric calibration).

[f] Blue tube attenuates strongly above 5500Å.

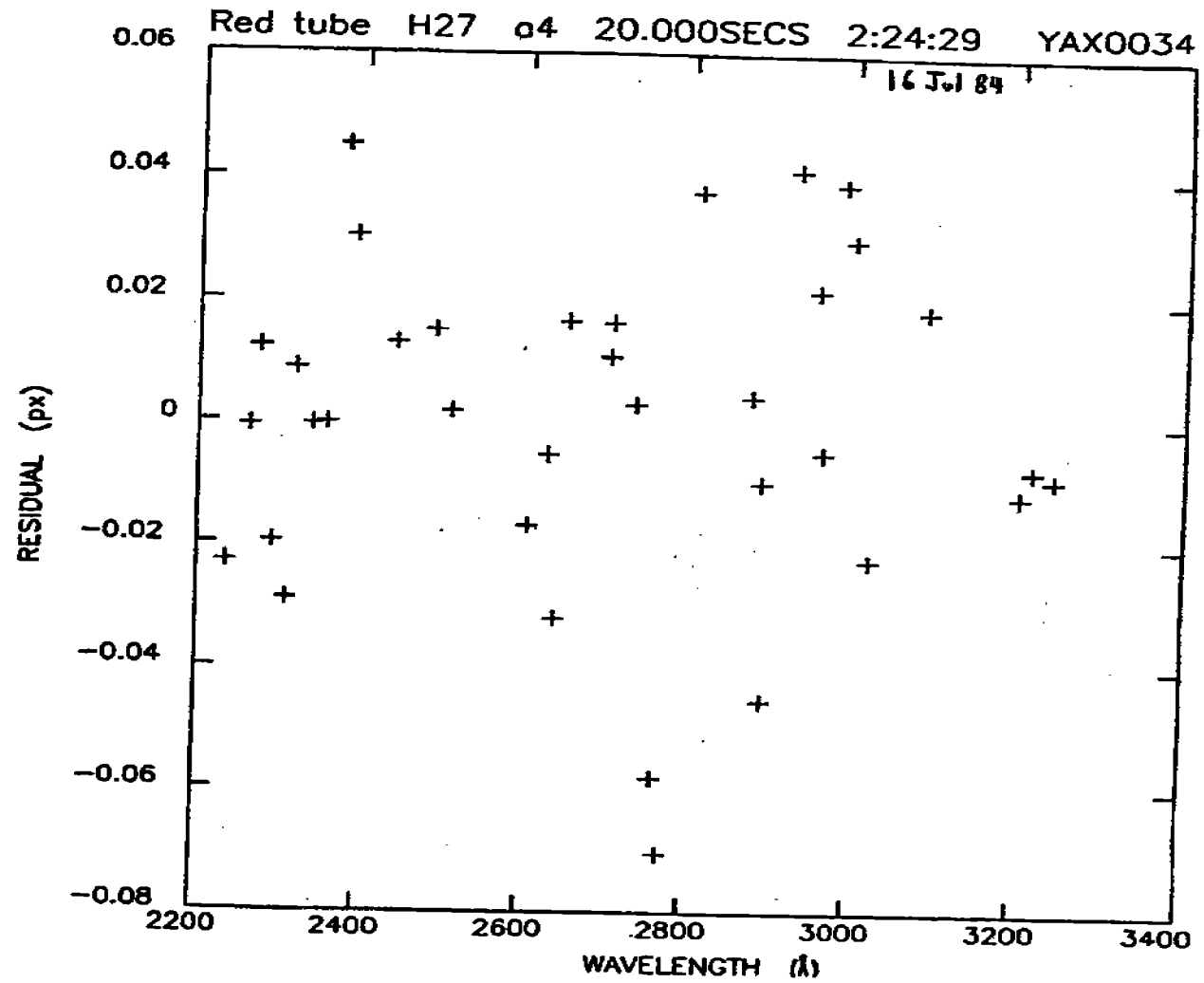

Figure 5.1-3. Plot of residuals for a cubic fit vs. wavelength for H27, red Digicon. Here the residuals seem fairly randomly distributed with the majority confined to ± .04 pixels.